PLOS ONE

RESEARCH ARTICLE

A quantitative systems pharmacology approach, incorporating a novel liver model, for predicting pharmacokinetic drug-drug interactions

Mohammed H. Cherkaoui-Rbati[1]*, Stuart W. Paine[1], Peter Littlewood[2], Cyril Rauch[1]

1 School of Veterinary Medicine and Science, University of Nottingham, Sutton Bonington, Leicestershire, United Kingdom, **2** Vertex Pharmaceuticals (Europe) Limited, Abingdon, Oxfordshire, United Kingdom

* mohammed.h.cherkaoui@gmail.com

Check for updates

OPEN ACCESS

Citation: Cherkaoui-Rbati MH, Paine SW, Littlewood P, Rauch C (2017) A quantitative systems pharmacology approach, incorporating a novel liver model, for predicting pharmacokinetic drug-drug interactions. PLoS ONE 12(9): e0183794. https://doi.org/10.1371/journal.pone.0183794

Editor: Jinn-Moon Yang, National Chiao Tung University College of Biological Science and Technology, TAIWAN

Received: November 30, 2016

Accepted: August 11, 2017

Published: September 14, 2017

Copyright: © 2017 Cherkaoui-Rbati et al. This is an open access article distributed under the terms of the Creative Commons Attribution License, which permits unrestricted use, distribution, and reproduction in any medium, provided the original author and source are credited.

Data Availability Statement: All relevant data are within the paper and its Supporting Information files.

Funding: The funder, Vertex Pharmaceutical, provided support in the form of PhD sponsoring for MHCR and welcomed MHCR in their offices for 6 months to conduct his experiments, where PL was supervising him. Furthermore, PL was attending in a regular basis meetings at the

Abstract

All pharmaceutical companies are required to assess pharmacokinetic drug-drug interactions (DDIs) of new chemical entities (NCEs) and mathematical prediction helps to select the best NCE candidate with regard to adverse effects resulting from a DDI before any costly clinical studies. Most current models assume that the liver is a homogeneous organ where the majority of the metabolism occurs. However, the circulatory system of the liver has a complex hierarchical geometry which distributes xenobiotics throughout the organ. Nevertheless, the lobule (liver unit), located at the end of each branch, is composed of many sinusoids where the blood flow can vary and therefore creates heterogeneity (*e.g.* drug concentration, enzyme level). A liver model was constructed by describing the geometry of a lobule, where the blood velocity increases toward the central vein, and by modeling the exchange mechanisms between the blood and hepatocytes. Moreover, the three major DDI mechanisms of metabolic enzymes; competitive inhibition, mechanism based inhibition and induction, were accounted for with an undefined number of drugs and/or enzymes. The liver model was incorporated into a physiological-based pharmacokinetic (PBPK) model and simulations produced, that in turn were compared to ten clinical results. The liver model generated a hierarchy of 5 sinusoidal levels and estimated a blood volume of 283 mL and a cell density of 193×10^6 cells/g in the liver. The overall PBPK model predicted the pharmacokinetics of midazolam and the magnitude of the clinical DDI with perpetrator drug(s) including spatial and temporal enzyme levels changes. The model presented herein may reduce costs and the use of laboratory animals and give the opportunity to explore different clinical scenarios, which reduce the risk of adverse events, prior to costly human clinical studies.

Introduction

A pharmacokinetic drug-drug interaction (DDI) is where a drug(s), the perpetrator drug(s), interacts with a metabolizing enzyme(s) or membrane transporter(s) such that the

University of Nottingham from the conceptualization to the validation of the PhD. Finally he was also part of the review of this manuscript. This does not alter our adherence to PLOS ONE policies on sharing data and materials.

Competing interests: There are no patents, products in development or marketed products to declare. SWP and CR received a grant from Vertex Pharmaceutical (http://www.vrtx.com/) for a PhD sponsorship. This sponsoring does not alter our adherence to PLOS ONE policies on sharing data and materials.

pharmacokinetics (PK) of another drug(s), the victim drug(s), is altered. In the late 1970s, the first cases of pharmacokinetic DDIs were reported [1], and since then more and more DDIs have been identified especially in the situation of polypharmacy as is often the case for elderly patients [2]. The increase in observed DDIs coupled to some lethal cases [1] led the FDA to publish in 1997 the first *in vitro* metabolism drug interaction guidance document [3] for pharmaceutical companies. In order to identify the possible interactions of new chemical entities (NCEs), many strategies have been suggested as it is essential to know before costly clinical trials, whether a NCE will be a safe drug. One of those strategies relies on the combination of *in vitro* information coupled to mathematical models to predict the clinical DDIs. This has the advantage to be cost effective, reduce the use of laboratory animals and give the opportunity to explore different clinical scenarios in order to identify optimum dose regimens. Excluding the limitations of *in vitro* experiments, the modeling approach is limited by the sophistication of the implemented models. Current models are classified into two different categories that depend on whether they are a function of time or not (*i.e.* static and dynamic models), and mainly focus on one enzyme and/or one particular aspect of DDIs (*e.g.* reversible inhibition [4], mechanism based inhibition [5] or induction [6]). In their most advanced form the static models may account for all kinds of DDIs [7], but are limited in their ability to describe complex mechanisms related to administration, distribution, metabolism or excretion such as active drug transport (uptake) into hepatocytes or enterocytes. Although the dynamic models are more descriptive, traditionally, the dynamic models were developed to describe specific drug cases [4, 5, 8] and most of them assume that the liver is a homogeneous organ (*e.g.* well-stirred model [9, 10]) where the majority of the metabolism occurs. However, the circulatory system of the liver has a complex hierarchical geometry which helps to distribute xenobiotics throughout the organ. Nevertheless, the lobule (liver unit), located at the end of each branch, is composed of many sinusoids (small blood vessels) where the blood flow can vary and therefore creates heterogeneity (*e.g.* drug concentration, enzyme level). Some liver models account for heterogeneity, such as the parallel tube model [9, 10] and the dispersion model [11, 12], but they have not been used to predict DDIs and do not account for the variation in blood flow through the lobules. With established methodologies of *in vitro* screening for DDIs, pharmaceutical companies need adequate tools to predict the net result of *in vivo* DDIs to translate their *in vitro* observations to clinical predictions. It is common for elderly patients to receive several medications to treat different symptoms or conditions. Each of these medicines can potentially interfere with the usual routes of metabolism for another drug. There is a serious need for better models to cover all different scenarios, which also takes into account the variabilities between individuals, such as size, weight and differences in genetic polymorphisms [13]. In this paper, a liver model will be presented that takes into account three major DDI mechanisms of metabolic enzymes; competitive inhibition, mechanism based inhibition (MBI) and induction, with an undefined number of drugs and/or enzymes, where the lobule geometry will be accounted for due to its impact on blood flow heterogeneity. The liver model will then be incorporated into a physiological-based pharmacokinetic (PBPK) model and simulations produced that in turn will be compared to clinical results. The description of the model proposed herein is divided into six parts. The first part will introduce the model and the notations used throughout the document including a new liver model taking into consideration its hierarchical structure and the different body compartments that are essential to drug metabolism. In the second part, the algorithm to generate the lobule geometry will be presented, where length and radius of the sinusoids are produced. In the third part, the transport and metabolism reactions of the drugs will be mathematically described. As the drugs are distributed in the body through the bloodstream, the conservation equation will be used in the liver sinusoids to describe the blood transport and the exchange mechanisms between the

blood and hepatocytes, such as passive diffusion and active uptake/efflux of the drugs. Inside the hepatocytes, drug metabolism and drug interactions with metabolic enzymes will be described. In the fourth part, the PBPK model presented in part one will be fully developed. In part five, a brief description on how the PBPK was numerically resolved will be given. In the sixth part, drugs for which data exist will be considered and their physiological parameters defined. Finally the results from the new liver model will be presented and compared to clinical data.

Models

Presentation of the liver model and notations

The objective of this section is to provide a brief explanation of the subsequent models that will be used to develop a formal understanding of DDIs. There are three major aspects to consider; (i) the geometry of the lobule (ii) the set of complex interactions between xenobiotics and enzymes (iii) the usual set of body compartments (PBPK Model).

Drugs move with the flow of blood and as a result the exchange mechanisms of drug between the blood and the tissue will be a function of the lobule geometry in which the flow takes place. The lobules have a peculiar shape idealized as hexagons composed of a series of peripheral entries (portal veins and hepatic arteries) and a central vein (Fig 1A and 1B). This spatial configuration and its hierarchical structure will need to be taken into consideration in order to describe the blood flow and to generate an algorithm to construct a lobule within the physiological constraints. Furthermore, the blood velocity will be assumed constant and averaged over the cross section of sinusoids present within the lobule while it will vary along the length of sinusoids as their radii narrow. The latter assumption is the only one that will be used, which reduces the spatial dimension to one. The spatial variable is noted x and for each sinusoids portion the x-axis is taken along the bisector and goes from the external part of the lobule to the central vein (Fig 1C).

To describe the DDIs no assumptions will be made on the number of drugs and enzymes involved to make the model generic for all animal species. However, the only way to achieve this is to consider matrix calculus. While this may appear as an unnecessary complication at first sight, it will be seen that with adequately defined operators the writing of equations is largely intuitive even for those not fully familiar with matrix algebra. To start with, the following notations n_C and n_E will refer to the number of drugs and enzymes, respectively. To distinguish between scalars and matrices (including vectors), matrices and vectors are written in bold. Thus any set of variables or constants related to drugs shall be described as a column vector of size n_C including their concentrations: $\boldsymbol{C} = (C_1 \cdots C_{n_C})^{tr}$ or membrane permeability: $\boldsymbol{P} = (P_1 \cdots P_{n_C})^{tr}$. Note here that the subscript "tr" refers to the transposition of a column vector into a vector line (the same notation shall be used for matrices where in this case the operator transposed is noted: $\boldsymbol{A}^{tr} = (a^{tr}_{i,j})_{\substack{1 \le i \le m \\ 1 \le j \le n}} = (a_{j,i})_{\substack{1 \le i \le m \\ 1 \le j \le n}}$ where $\boldsymbol{A} = (a_{i,j})_{\substack{1 \le i \le n \\ 1 \le j \le m}}$). Similarly, any set of variables or constants related to enzymes or their degradation shall be described as a column vector of size n_E including for example the enzyme concentrations: $\boldsymbol{E} = (E_1 \cdots E_{n_E})^{tr}$; or their degradation: $\boldsymbol{k_{deg}} = (k_{deg,\,1} \cdots k_{deg,\,n_E})^{tr}$. As the number of possible pair interactions between enzymes and drugs is given by the scalar product: $n_C \times n_E$, one defines the matrix $\boldsymbol{EC} = (EC_{i,j})_{\substack{1 \le i \le n_C \\ 1 \le j \le n_E}}$ where the term $EC_{i,\,j}$ represents the interaction of the i-th drug with the j-th enzyme. Finally, as the interaction between the i-th drug with the j-th enzyme can lead to the formation of a product one needs to specify the kinetics of the reaction by another parameter, $k_{cat,\,i,\,j}$, specific to the $EC_{i,\,j}$ complex. In these conditions the scalar product $k_{cat,\,i,\,j} \times EC_{i,\,j}$

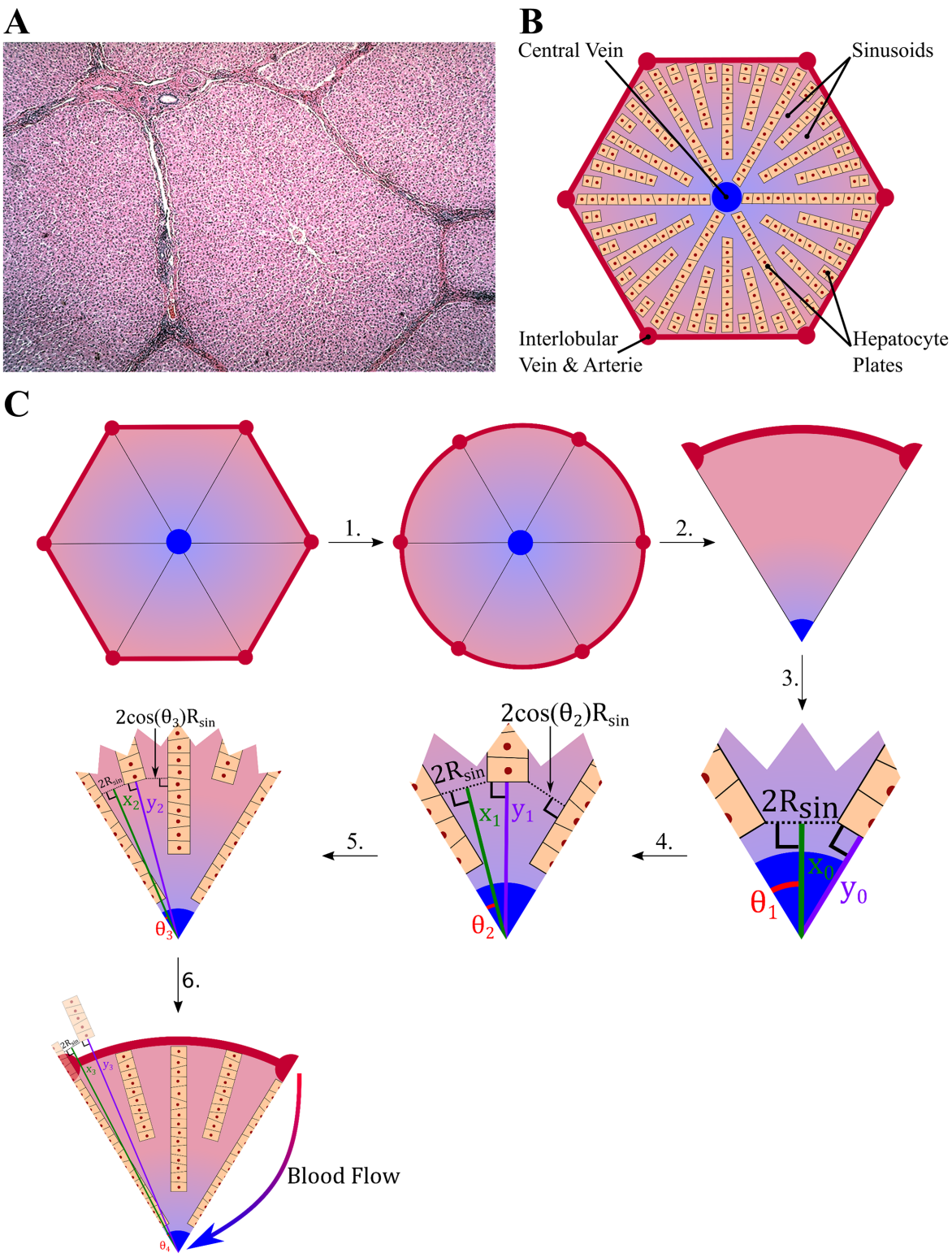

Fig 1. Lobule geometry and modelling. (A) The lobule cross section as represented displays an apparent elementary symmetry essential for its physiology primarily given by the blood vessels and the blood flow (Credit to Dr. Roger C. Wagner, University of Delaware). (B) This symmetry is used when lobule modeling or representation are involved. In general, a lobule is represented by a hexagon composed of hepatocyte plates. These plates are hierarchically organized to optimize exchanges. (C) To model the blood flow (and subsequent exchanges between the liver tissues and the blood), an algorithm was designed to

automatically generate the length and radius of the sinusoids. The latter is used to estimate the changes in velocity within a sinusoid portion by assuming a constant blood flow and a constant velocity over the cross section.

https://doi.org/10.1371/journal.pone.0183794.g001

define the reaction rate of the reaction. To use matrices one needs to define the following operators: "·" such that $\boldsymbol{k_{cat}} \cdot \boldsymbol{EC} = (k_{cat,i,j} \times EC_{i,j})_{\substack{1 \le i \le n_C \\ 1 \le j \le n_E}}$. By extension, a division operator is defined and noted "/" or "–" between vectors or matrices such that: $\boldsymbol{x}/\boldsymbol{y} = \frac{\boldsymbol{x}}{\boldsymbol{y}} = \left(\frac{x_{i,j}}{y_{i,j}}\right)_{\substack{1 \le i \le n \\ 1 \le j \le m}}$.

Finally for completion the column vectors of size n_C or n_E and of components equal to unity shall be noted: $\mathbb{1}_{n_C}$ and $\mathbb{1}_{n_E}$.

Last but not least, a seven-compartment model is used involving: venous blood, arterial blood, liver, gut, kidneys, lungs (to consider the pulmonary circulation), and the rest of the body (Fig 2). The average volume and blood flow of each compartment is given in S1 Table.

Lobule geometry

The lobule is the elementary unit of the liver where the exchange of nutrients and xenobiotic compounds occurs between the blood and the hepatocytes. The shape of the lobule and the spatial distribution of the hepatocytes are irregular in appearance (Fig 1A). But schematically, the liver lobule can be represented by a hexagon (Fig 1B), where the hepatic vein is at the centre and where at each apex, the hepatic artery and the hepatic portal vein pour blood into the sinusoids. The sinusoids are converging toward the centre where the blood leaves the lobule through the central vein (Fig 1B).

To suggest a theory on which an amenable model will be based, the lobule geometry will be simplified. The parameters used to define the geometry are summarized in Table 1, whereas the algorithm to build the lobule geometry for the simulations is schematically represented in Fig 1C where each step is numbered and detailed as below:

1. The hexagonal shape of the lobule is replaced by a disc of similar area: $\frac{3\sqrt{3}}{2}\overline{R}^2_{lobule} = \pi R^2_{Circle}$.
2. Due to the symmetry of an hexagon, only one sixth of the circle will be taken into account.
3. The initial two hepatocyte plates are placed on either edge of the sector (one sixth of the circle) and respect a minimal distance of $2R_{Sin}$ between the hepatocytes plates, the initial distances from the centre are estimated by:
   a. The first sinusoid output: $x_0 = \frac{R_{Sin}}{\tan\theta_1} + \frac{e}{2\sin\theta_1}$ where $\theta_k = \frac{\theta_0}{2^k}$ and $\theta_0 = 60°$.
   b. The first hepatocyte plate: $y_0 = \frac{R_{Sin}}{\sin\theta_1} + \frac{e}{2\tan\theta_1}$.
   c. Iteration initialization: $k = 0$
4. A loop is implemented as follow: while $x_k \le R_{Circle}$ do
   a. $k = k + 1$
   b. Place a hepatocyte plate on each line of angle $\theta_k + (i-1)\theta_{k-1}$ for $\forall i \in \{1, \ldots, 2^{k-1}\}$, such as the minimal distance of the new hepatocyte plate to the previous one is $2R_{Sin}\cos\theta_{k+1}$, which gives an output diameter of $2R_{Sin}$.
   c. The distance of the outputs: $x_k = \frac{R_{Sin}}{\tan\theta_{k+1}} + \frac{e}{2\sin\theta_{k+1}}$.

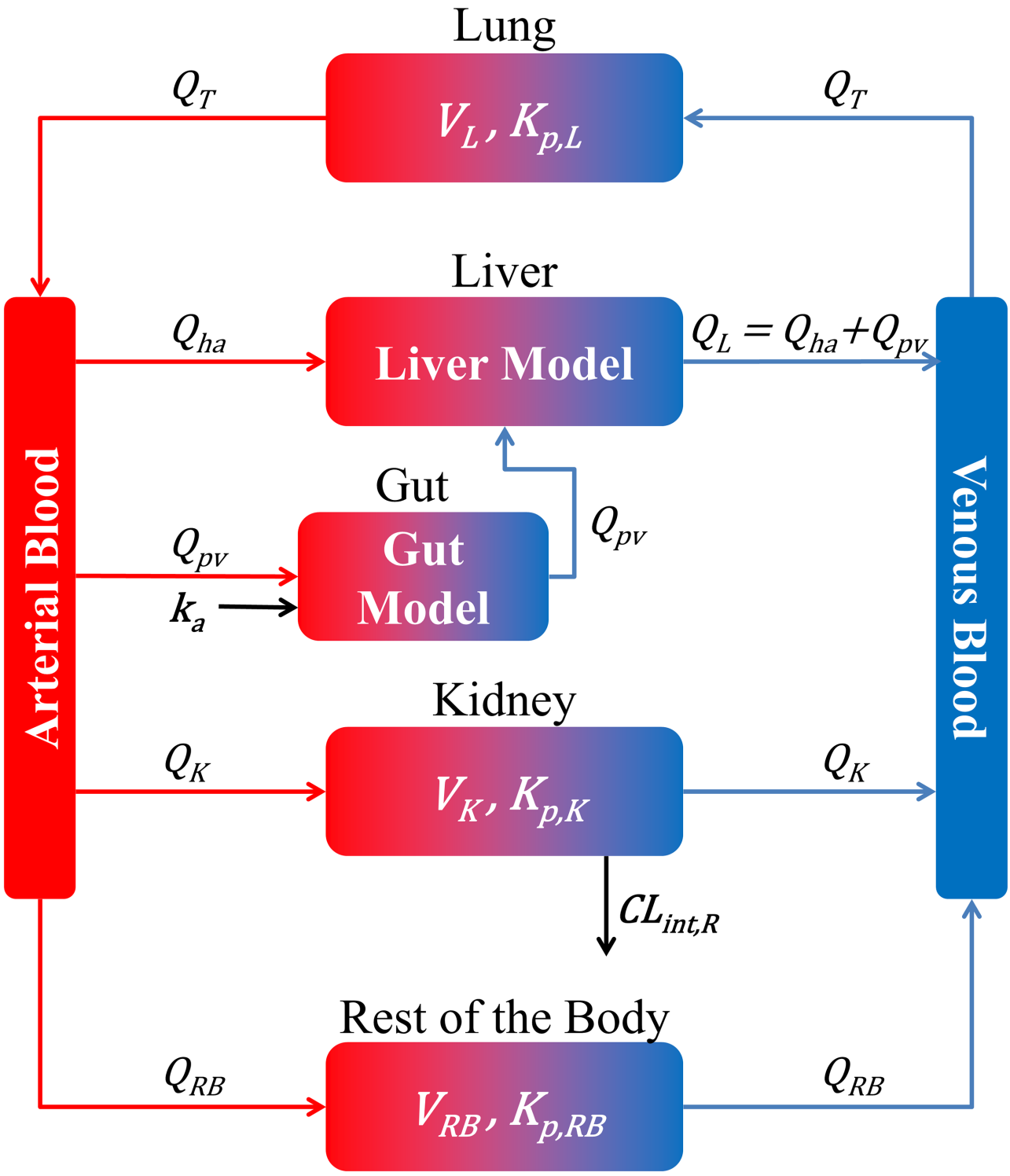

Fig 2. The seven compartmental model. Red and blue arrows represent blood flows (Q_i where i represents: T for total blood flow, ha hepatic artery blood flow, pv portal vein blood flow, L for the liver blood flow, G for the gut blood flow, K for the kidneys blood flow and RB for the blood flow going to the rest of the body). The black arrows represent absorption (k_a: absorption constant rate) or excretion (CL_R: Renal Clearance).

https://doi.org/10.1371/journal.pone.0183794.g002

Table 1. Lobule parameters.

Parameter	Description	Value
R_{Lobule}	Lobule Radius	790.57μm [14]
R_{sin}	Minimal Sinusoidal Radius	3.65μm [14]
e_{Lobule}	Lobule Thickness	25.00μm [14]
R_H	Hepatocyte Radius	8.49μm [14]
e	Hepatocyte Plate Width(= $2R_H$)	16.97μm

https://doi.org/10.1371/journal.pone.0183794.t001

d. The distance of the new plates: $y_k = \frac{R_{Sin}}{\sin\theta_{k+1}} + \frac{e}{2\tan\theta_{k+1}}$.

5. When $x_k \geq \overline{R}_{Circle}$ the last level of sinusoid is reached and one poses $n = k$. Then in order to be consistent with the direction of the blood flow, the level 1 is defined as the furthest level from the central vein, and the level n as the closest one.

6. As a result, the length of each sinusoids level is given by: $L_k = \min(y_{n-k+1}, R_{Circle}) - x_{n-k}$.

Now that the number and the length of the sinusoid levels are defined, the radius within each level changes which is expected to impact the exchange of chemicals between the blood and the hepatocytes. Therefore it is essential to calculate the sinusoid radius changes for every level defined above. The radius along the sinusoids of level k, following the blood flow, is then given by:

$$R_k(x) = R_{Sin} + (L_k - x)\tan\theta_{n-k+1} \;\; \forall x \in [0 : L_k] \tag{1}$$

Finally, as one assumes that the blood flow Q_k at a given level k is identical for all sinusoids, the blood flow and the average velocity are given by:

$$\begin{cases} Q_k &= \dfrac{Q_{Lobule}}{6 \cdot 2^{n-k}} \\ v_k(x) &= \dfrac{Q_k}{\pi R_k(x)^2} \forall x \in [0 : L_k] \end{cases} \tag{2}$$

where the flow in a lobule is $Q_{Lobule} = Q_{Liver}/N_{Lobule}$ with $N_{Lobule} = V_{Liver}/V_{Lobule}$ and V_{Liver} and V_{Lobule} are, respectively, the liver and lobule volumes. This assumes the same flow in each lobule. Finally, to simplify the notation, in the remaining text we define:

$$\forall x \in [0 : \mathcal{L}_n]$$
$$\begin{cases} R(x) &= R_1(x)\mathbb{1}_{[\mathcal{L}_0:\mathcal{L}_1]} + \sum_{k=2}^{n} R_k(x - \mathcal{L}_{k-1}) I_{]\mathcal{L}_{k-1}:\mathcal{L}_k]}(x) \\ Q(x) &= Q_1(x)\mathbb{1}_{[\mathcal{L}_0:\mathcal{L}_1]} + \sum_{k=2}^{n} Q_k(x - \mathcal{L}_{k-1}) I_{]\mathcal{L}_{k-1}:\mathcal{L}_k]}(x) \\ v(x) &= v_1(x)\mathbb{1}_{[\mathcal{L}_0:\mathcal{L}_1]} + \sum_{k=2}^{n} v_k(x - \mathcal{L}_{k-1}) I_{]\mathcal{L}_{k-1}:\mathcal{L}_k]}(x) \end{cases} \tag{3}$$

where $\forall k \in [\![1 : n]\!] \;\; \mathcal{L}_k = \mathcal{L}_{k-1} + L_k$, $\mathcal{L}_0 = 0$ and I_E is the indicator function of E.

Conservation and kinetic equations for the liver model

Conservation equation in the blood. Now that the lobule geometry has been defined, the equations which describe the transport and metabolism of drugs in the liver can be expressed. Before being metabolized in the hepatocytes, the drugs flow with the blood through the lobules and are passively or actively transported into the hepatocytes. Considering n_C drugs and assuming no irreversible reaction within the blood, the conservation equation can be used to describe the concentrations such as:

$$\frac{\partial \boldsymbol{C_b}}{\partial t} + v(x)\frac{\partial \boldsymbol{C_b}}{\partial x} = -\alpha_{B\to H}(x)\left[(\boldsymbol{P}+\boldsymbol{\rho_{in}})\cdot \boldsymbol{f_u^b}\cdot \boldsymbol{C_b} - (\boldsymbol{P}+\boldsymbol{\rho_{out}})\cdot \boldsymbol{f_u^h}\cdot \boldsymbol{C_h}\right] \tag{4}$$

where $\boldsymbol{C_b}$, $\boldsymbol{C_h}$, $\boldsymbol{P}$, $\boldsymbol{\rho_{in}}$, $\boldsymbol{\rho_{out}}$, $\boldsymbol{f_u^b}$, $\boldsymbol{f_u^h}$ and $v(x)$ are, respectively, the concentrations of the drugs in the liver blood and hepatocytes, the permeability and the uptake/efflux rates through the hepatocyte membrane, the fraction unbound in the blood and hepatocytes and the blood velocity; and where $\alpha_{B\to H}(x)$ is the ratio of the elementary blood-hepatocyte surface exchange $\delta S_{Exchange}(x)$ to the elementary blood volume $\delta V_{Blood}(x)$ (see S1 Appendix), given by:

$$\alpha_{B\to H}(x) = \frac{2R(x) + \dfrac{e_L - 2R_H}{\cos\theta(x)}}{R(x)(e_L - 2R_H)} \tag{5}$$

As the blood flow enters the sinusoid from the hepatic arteries at $x = 0$, the initial and boundary conditions are given by:

$$\begin{cases} \boldsymbol{C_b}(x>0, t=0) = 0 \\ \boldsymbol{C_b}(x=0, t) = \boldsymbol{C}_0(t) \\ \boldsymbol{C_h}(x, t=0) = 0 \end{cases} \tag{6}$$

where $C_0(t)$ will be defined once the PBPK model will be decribed.

Drug kinetic equation in the hepatocytes. Once the drugs enter inside the hepatocytes by passive and/or active transport, a cascade of reactions may occur involving metabolism of the drugs by one or more enzymes and includes cross reaction(s) between metabolite(s) and drug(s). The presented model focuses specifically on the reactions schematically represented in Fig 3 (*i.e.* Competitive Inhibition, MBI and Induction).

Furthermore, it will be assumed that no exchange of materials between hepatocytes happens and that the equilibrium between the drugs and enzyme complex is quickly reached (see S2 Appendix for the mathematical simplification). Therefore, by using the law of conservation of mass, one can describe the equation governing the concentration of drugs within the hepatocytes by:

$$\begin{aligned} \frac{d\boldsymbol{C_h}}{dt} = \; & \alpha_{H\to B}(x)[(\boldsymbol{P}+\boldsymbol{\rho_{in}})\cdot \boldsymbol{f_u^b}\cdot \boldsymbol{C_b} - (\boldsymbol{P}+\boldsymbol{\rho_{out}})\cdot \boldsymbol{f_u^h}\cdot \boldsymbol{C_h}] \\ & -(\boldsymbol{k_{cat}}\cdot \boldsymbol{EC_{Met}})\mathbb{1}_{n_E} \\ & -(\boldsymbol{k_{inact}}\cdot \boldsymbol{EC_{MBI}})\mathbb{1}_{n_E} \\ & -\frac{\boldsymbol{V_{max,2}}}{\boldsymbol{K_{m,2}} + \boldsymbol{f_u^h}\cdot \boldsymbol{C_h}}\cdot \boldsymbol{f_u^h}\cdot \boldsymbol{C_h} \end{aligned} \tag{7}$$

where $\boldsymbol{EC_{Met}} = (EC_{Met,i,j})_{\substack{1\le i\le n_C \\ 1\le j\le n_E}}$ represents the concentration of complex involved in the

- Metabolism:

$$E + C \underset{k_{21}}{\overset{k_{12}}{\rightleftharpoons}} EC_{Met} \xrightarrow{k_{cat}} E + P$$

- Competitive Inhibition:

$$E + C \underset{k_{31}}{\overset{k_{13}}{\rightleftharpoons}} EC_{Inh}$$

- Mechanism Based Inhibition:

$$E + C \underset{k_{41}}{\overset{k_{14}}{\rightleftharpoons}} EC_{MBI} \xrightarrow{k_{inact}} EC^{*}_{MBI}$$

- Induction:

$$C \overset{FI_{\max}, EC_{50}}{\rightsquigarrow} E$$

Fig 3. Enzymatic reactions taken into account in the liver model. Reversible inhibition: A drug binds to an enzyme which may result in its metabolism (but not necessarily) resulting in the temporary blockade or inhibition of the enzyme. Here only competitive inhibition will be studied, which assumes that each enzyme can interact with one drug at a time. Mechanism Based Inhibition (MBI): A drug inactivates an enzyme through direct interaction resulting in an inhibited metabolism of any drug metabolized by these enzymes. Induction: A drug induces the expression of one or more enzymes resulting in an induced metabolism of any drug metabolized by these enzymes. Note that the notations in this figure regarding the kinetic rate constants are used in the text.

https://doi.org/10.1371/journal.pone.0183794.g003

metabolism of drugs, $\boldsymbol{EC_{MBI}} = (EC_{MBI,i,j})_{\substack{1 \le i \le n_C \\ 1 \le j \le n_E}}$ the concentration of complex inactivating the enzymes and; $\boldsymbol{V_{max,\,2}}$ and $\boldsymbol{K_{m,\,2}}$ the constants associated with unspecified metabolic pathway (s), modeled by a Michaelis-Menten equation. Finally $\alpha_{H \to B}(x)$ is the ratio of the elementary blood-hepatocyte surface exchange $\delta S_{Exchange}(x)$ to the elementary hepatocyte volume $\delta V_{Hep}(x)$ (see S1 Appendix), given by:

$$\alpha_{H \to B}(x) = \frac{2R(x) + \dfrac{e_L - 2R_H}{\cos\theta}}{R_H\left(2R_k(x) + \dfrac{e_L}{\cos\theta}\right)} \tag{8}$$

Eq (7) can be rewritten considering the rapidly attained equilibrium assumption. In this context the enzyme-drug complex concentrations can be expressed as a function of the free

enzyme levels and drug concentrations as follow:

$$\begin{aligned} \boldsymbol{EC}_{Met} &= \frac{(\boldsymbol{f}_u^h \cdot \boldsymbol{C}_h)\boldsymbol{E}^{tr}}{\boldsymbol{K}_{m,1}} \\ \boldsymbol{EC}_{MBI} &= \frac{(\boldsymbol{f}_u^h \cdot \boldsymbol{C}_h)\boldsymbol{E}^{tr}}{\boldsymbol{K}_I} \end{aligned} \tag{9}$$

where $\boldsymbol{E} = (E_1, \ldots, E_{n_E})^{tr}$ represents the free enzyme levels and where the constants $\boldsymbol{K}_{m,1} = \frac{\boldsymbol{k}_{21} + \boldsymbol{k}_{cat}}{\boldsymbol{k}_{12}}$ and $\boldsymbol{K}_I = \frac{\boldsymbol{k}_{41} + \boldsymbol{k}_{inact}}{\boldsymbol{k}_{14}}$ are developed in S2 Appendix. Therefore the equation becomes:

$$\begin{aligned} \frac{d\boldsymbol{C}_h}{dt} = \quad & \alpha_{HB}(x)[(\boldsymbol{P} + \boldsymbol{\rho}_{in}) \cdot \boldsymbol{f}_u^b \cdot \boldsymbol{C}_b - (\boldsymbol{P} + \boldsymbol{\rho}_{out}) \cdot \boldsymbol{f}_u^h \cdot \boldsymbol{C}_h] \\ & - \left[\left(\boldsymbol{k}_{cat}/\boldsymbol{K}_{m,1} + \boldsymbol{k}_{inact}/\boldsymbol{K}_I\right)\boldsymbol{E}\right] \cdot \boldsymbol{f}_u^h \cdot \boldsymbol{C}_h - \frac{\boldsymbol{V}_{max,2}}{\boldsymbol{K}_{m,2} + \boldsymbol{f}_u^h \cdot \boldsymbol{C}_h} \cdot \boldsymbol{f}_u^h \cdot \boldsymbol{C}_h \end{aligned} \tag{10}$$

Enzyme kinetic equation in the hepatocytes. The remaining set of equations needs to describe the enzyme kinetics. In general the level of enzymes are assumed to be constant, but when MBI and/or induction occur, changes in enzyme levels are not immediate and time needs to be taken into consideration. Therefore modelling the enzyme kinetics is essential, using classical kinetic equations and assuming that the enzyme induction is additive, the following can be written:

$$\begin{cases} \dfrac{d\boldsymbol{E}_{Tot}}{dt} \approx \dfrac{d\boldsymbol{E}}{dt} = \quad \boldsymbol{k}_{deg} \cdot \left[\boldsymbol{E}_0 + \left(\dfrac{\boldsymbol{E}_{max} - \mathbb{1}_{n_C}\boldsymbol{E}_0^{tr}}{\boldsymbol{EC}_{50} + (\boldsymbol{f}_u^h \cdot \boldsymbol{C}_h)\mathbb{1}_{n_E}^{tr}}\right)^{tr} (\boldsymbol{f}_u^h \cdot \boldsymbol{C}_h) - \boldsymbol{E}_{Tot}\right] \\ \qquad\qquad\qquad\qquad - (\boldsymbol{k}_{inact} \cdot \boldsymbol{EC}_{MBI})^{tr}\mathbb{1}_{n_C} \\ \dfrac{d\boldsymbol{EC}_{Met}}{dt} = \dfrac{d\boldsymbol{EC}_{Inh}}{dt} = \dfrac{d\boldsymbol{EC}_{MBI}}{dt} \approx 0 \\ \boldsymbol{E}_{Tot} = \boldsymbol{E} + [\boldsymbol{EC}_{Met} + \boldsymbol{EC}_{Inh} + \boldsymbol{EC}_{MBI}]^{tr}\mathbb{1}_{n_C} \end{cases} \tag{11}$$

where $\boldsymbol{EC}_{Inh} = (EC_{Inh,i,j})_{\substack{1 \le i \le n_C \\ 1 \le j \le n_E}}$ is the concentration(s) of complex that does not metabolize the drugs and is also given by $\boldsymbol{EC}_{Inh} = \frac{(\boldsymbol{f}_u^h \cdot \boldsymbol{C}_h)\boldsymbol{E}^{tr}}{\boldsymbol{K}_i}$ where $\boldsymbol{K}_i = \frac{\boldsymbol{k}_{31}}{\boldsymbol{k}_{13}}$ (see S2 Appendix). The equation above can be further simplified by using Eq (9) and by normalizing the enzyme levels by its initial and basal level E_0 and by noting $\bar{\boldsymbol{E}}_{Tot} = \boldsymbol{E}_{Tot}/\boldsymbol{E}_0$ and $\boldsymbol{FI}_{max} = \boldsymbol{E}_{max}/(\mathbb{1}_{n_C}\boldsymbol{E}_0^{tr})$:

$$\begin{cases} \dfrac{d\bar{\boldsymbol{E}}_{Tot}}{dt} = \boldsymbol{k}_{deg} \cdot \left[1 + \left(\dfrac{(\boldsymbol{FI}_{max} - 1)}{\boldsymbol{EC}_{50} + (\boldsymbol{f}_u^h \cdot \boldsymbol{C}_h)\mathbb{1}_{n_E}^{tr}}\right)^{tr} (\boldsymbol{f}_u^h \cdot \boldsymbol{C}_h) - \bar{\boldsymbol{E}}_{Tot} \cdot \left(1 + \dfrac{\dfrac{1}{\boldsymbol{k}_{deg}} \cdot \left(\dfrac{\boldsymbol{k}_{inact}}{\boldsymbol{K}_I}\right)^{tr} (\boldsymbol{f}_u^h \cdot \boldsymbol{C}_h)}{1 + \left(\dfrac{1}{\boldsymbol{K}_{m,1}} + \dfrac{1}{\boldsymbol{K}_i} + \dfrac{1}{\boldsymbol{K}_I}\right)^{tr} (\boldsymbol{f}_u^h \cdot \boldsymbol{C}_h)}\right)\right] \\ \bar{\boldsymbol{E}} = \dfrac{\bar{\boldsymbol{E}}_{Tot}}{1 + \left(\dfrac{1}{\boldsymbol{K}_{m,1}} + \dfrac{1}{\boldsymbol{K}_i} + \dfrac{1}{\boldsymbol{K}_I}\right)^{tr} (\boldsymbol{f}_u^h \cdot \boldsymbol{C}_h)} \end{cases} \tag{12}$$

Note that if a drug is not metabolized or does not bind or inactivate a specific enzyme, the related constant is set to infinity, which corresponds to an infinite potency. Furthermore, it is important to note that if two drugs are metabolized by the same enzyme site they automatically inhibit each other and as a result $\boldsymbol{K_i}$ can be taken as infinity, except if it is suspected that two binding sites are active for a given drug (*e.g.* one will metabolize the drug whereas the other will just bind to it). However it is difficult to make this distinction experimentally.

PBPK model

Having the liver model defined and the related enzymatic reactions, they need to be incorporated into a PBPK model to be able to simulate the PK of the different drugs and predict their interactions. As seen above, the PBPK model is constituted of 7 compartments: Arterial Blood, Venous Blood, Liver, Gut, Kidneys, Lungs and the Rest of the Body (RB) (Fig 2). All compartments, except the liver and gut, are modeled below as classical compartments associated with their own physiological volume and partition coefficient for drugs [15]. Furthermore, as the drug(s) is(are) administered orally at $t = 0$ the initial concentration of all compartments is taken equal to zero. Finally, each of the compartments is defined as:

- Arterial Blood Compartment:

$$V_{AB}\frac{d\boldsymbol{C_{AB}}}{dt} = Q_T\left(\frac{\boldsymbol{C_{Lungs}}\cdot\boldsymbol{R_{BP}}}{\boldsymbol{K_{p,Lungs}}} - \boldsymbol{C_{AB}}\right) \tag{13}$$

  where $\boldsymbol{C_{AB}}$ and V_{AB} are the concentration of drugs and volume of the arterial blood, Q_T the total blood flow and $\boldsymbol{C_{Lungs}}$ and $\boldsymbol{K_{p,\,Lungs}}$ the concentration and partition coefficient of the lungs; and $\boldsymbol{R_{BP}}$ the blood-to-plasma ratio.

- Venous Blood Compartment:

$$V_{VB}\frac{d\boldsymbol{C_{VB}}}{dt} = Q_{Liver}\boldsymbol{C_{Liver}} + Q_K\frac{\boldsymbol{C_K}\cdot\boldsymbol{R_{BP}}}{\boldsymbol{K_{p,K}}} + Q_{RB}\frac{\boldsymbol{C_{RB}}\cdot\boldsymbol{R_{BP}}}{\boldsymbol{K_{p,RB}}} - Q_T\boldsymbol{C_{VB}} \tag{14}$$

  where $\boldsymbol{C_{VB}}$ and $\boldsymbol{V_{VB}}$ are the concentration of drugs and volume of the venous blood compartment, $\boldsymbol{C_{Liver}}$ and Q_{Liver} are the concentration of drugs and blood flow for the liver and where, $\boldsymbol{C_K}$, $\boldsymbol{C_{RB}}$, Q_K, Q_{RB}, $\boldsymbol{K_{p,\,K}}$ and $\boldsymbol{K_{p,\,RB}}$, $\boldsymbol{C_{Liver}}$ are the concentrations of drugs, the blood flows and partition coefficients of the kidney and the compartment corresponding to the rest of the body (RB-compartment), respectively. To be more specific $\boldsymbol{C_{Liver}}$ is the concentration at the exit of the lobule.

- Kidney Compartment:

$$V_K\frac{d\boldsymbol{C_K}}{dt} = Q_K\left(\boldsymbol{C_{AB}} - \frac{\boldsymbol{C_K}\cdot\boldsymbol{R_{BP}}}{\boldsymbol{K_{p,K}}}\right) - \boldsymbol{CL_{int,R}}\cdot\boldsymbol{C_K} \tag{15}$$

  where $\boldsymbol{CL_{int,\,R}}$ is the intrinsic renal clearance.

- Lung Compartment:

$$V_{Lungs}\frac{d\boldsymbol{C_{Lungs}}}{dt} = Q_{Lungs}\left(\boldsymbol{C_{VB}} - \frac{\boldsymbol{C_{Lungs}}\cdot\boldsymbol{R_{BP}}}{\boldsymbol{K_{p,Lungs}}}\right) \tag{16}$$

  where V_{Lungs} and Q_{Lungs} are the volume of the lungs and blood flow in the lungs, respectively.

- RB-Compartment:

$$V_{RB}\frac{d\boldsymbol{C_{RB}}}{dt} = Q_{RB}\left(\boldsymbol{C_{AB}} - \frac{\boldsymbol{C_{RB}}\cdot\boldsymbol{R_{BP}}}{\boldsymbol{K_{p,RB}}}\right) \tag{17}$$

- Gut Compartment:
The gut compartment is composed of two sub-compartments [16]; the gut wall and the portal vein sub-compartments (Fig 4). The model to describe the gut wall sub-compartment is similar to the liver model with a few differences including a homogeneous compartment with a first order absorption, differences in enzyme levels and convection to the portal vein. Therefore the concentration of drugs and enzymes within the gut wall are described by:

$$\begin{cases} \dfrac{d\boldsymbol{C_g}}{dt} = & \displaystyle\sum_{i=1}^{n_{Dose}} \frac{\boldsymbol{F_a}\cdot\boldsymbol{D_i}\cdot\boldsymbol{k_a}}{V_g}\cdot\exp(-\boldsymbol{k_a}(t-T_i))H(t-T_i) \\ & -[(\boldsymbol{k^g_{cat}}/\boldsymbol{K^g_{m,1}} + \boldsymbol{k^g_{inact}}/\boldsymbol{K^g_I})\boldsymbol{E_g}]\cdot\boldsymbol{f^g_u}\cdot\boldsymbol{C_g} \\ & -\dfrac{\boldsymbol{V^g_{max,2}}}{\boldsymbol{K^g_{m,2}}+\boldsymbol{f^g_u}\cdot\boldsymbol{C_h}}\cdot\boldsymbol{f^g_u}\cdot\boldsymbol{C_g} - \frac{Q_g}{V_g}\boldsymbol{f^g_u}\cdot\boldsymbol{C_g} \\ \dfrac{d\bar{\boldsymbol{E}}_{\boldsymbol{Tot,g}}}{dt} = \boldsymbol{k^g_{deg}} & \cdot\left[1+\left(\frac{(\boldsymbol{FI^g_{max}}-1)}{\boldsymbol{EC^g_{50}}+(\boldsymbol{f^g_u}\cdot\boldsymbol{C_g})\mathbb{1}^{tr}_{n_E}}\right)^{tr}(\boldsymbol{f^g_u}\cdot\boldsymbol{C_g}) - \bar{\boldsymbol{E}}_{\boldsymbol{Tot,g}}\cdot\left(\frac{1+\frac{1}{\boldsymbol{k^g_{deg}}}\cdot\left(\frac{\boldsymbol{k^g_{inact}}}{\boldsymbol{K^g_I}}\right)^{tr}(\boldsymbol{f^g_u}\cdot\boldsymbol{C_g})}{1+\left(\frac{1}{\boldsymbol{K^g_{m,1}}}+\frac{1}{\boldsymbol{K^g_i}}+\frac{1}{\boldsymbol{K^g_I}}\right)^{tr}(\boldsymbol{f^g_u}\cdot\boldsymbol{C_g})}\right)\right] \\ \bar{\boldsymbol{E}}_{\boldsymbol{g}} = \dfrac{\bar{\boldsymbol{E}}_{\boldsymbol{Tot,g}}}{1+\left(\frac{1}{\boldsymbol{K^g_{m,1}}}+\frac{1}{\boldsymbol{K^g_i}}+\frac{1}{\boldsymbol{K^g_I}}\right)^{tr}(\boldsymbol{f^g_u}\cdot\boldsymbol{C_g})} \end{cases} \tag{18}$$

where $\boldsymbol{C_g}$ is the concentration of drugs in the gut wall, $\boldsymbol{F_a}$ the fraction absorbed of the drugs, $\boldsymbol{D_i}$ the dose at time T_i, $\boldsymbol{k_a}$ the absorption rate constant of the drugs, n_{Dose} the total number of doses given, $\boldsymbol{f^g_u}$ the fraction of unbound drugs in the gut wall, V_g the volume of the gut wall, H the Heaviside function and $\bar{\boldsymbol{E}}_{\boldsymbol{g}}$ and $\bar{\boldsymbol{E}}_{\boldsymbol{Tot,g}}$ are the free and total normalized enzyme levels to the initial and basal enzyme level in the gut wall; $E_{0,g}$. Q_g is a hybrid parameter introduced by Yang [17], which takes into account the membrane permeability of the drugs and blood flow from the enterocytes to the portal vein (see S3 Appendix for more details). All other parameters, except $\boldsymbol{V^g_{max,2}}$ and $\boldsymbol{E_{0,g}}$, are taken equal to the corresponding liver values.
The concentration within the portal vein sub-compartment is given by:

$$\frac{d\boldsymbol{C_{pv}}}{dt} = \frac{Q_{pv}}{V_{pv}}\left(\boldsymbol{C_{AB}} - \boldsymbol{C_{pv}}\right) + \frac{Q_g}{V_{pv}}\cdot\boldsymbol{f^g_u}\cdot\boldsymbol{C_g} \tag{19}$$

where $\boldsymbol{C_{pv}}$ is the concentration in the portal vein, Q_{pv} the blood flow of the portal vein and V_{pv} the volume of the portal vein.

- Liver Compartment:
Finally the liver compartment is described by the liver model previously described with the boundary condition $\boldsymbol{C_0}(t) = \dfrac{Q_{ha}\boldsymbol{C_{AB}}(t) + Q_{pv}\boldsymbol{C_{pv}}(t)}{Q_{ha}+Q_{pv}}$ at $x = 0$ (Eq (6)). All volumes and

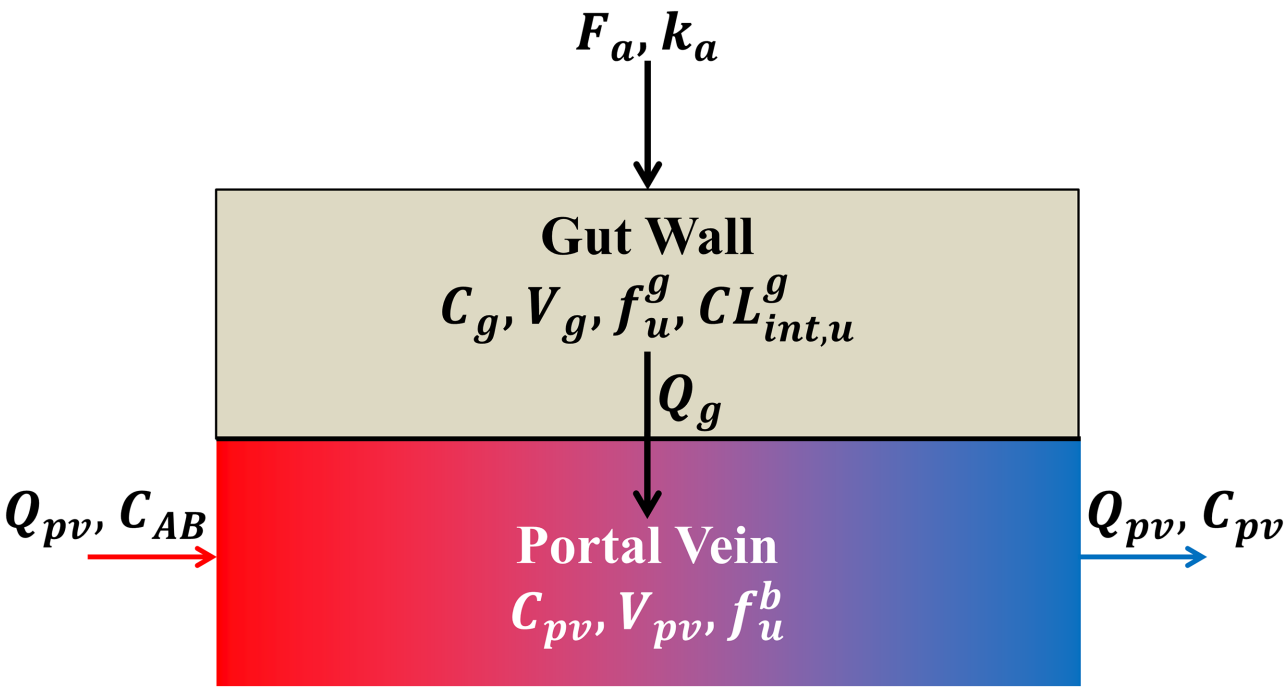

Fig 4. The gut-compartmental model. The gut compartment is composed of two sub-compartments; the gut wall and the portal vein sub-compartments. After an oral administration of a given drug, a fraction F_a is absorbed from the intestine to the gut wall with an absorption rate constant k_a. Once the drug is in the gut wall, it may be metabolized and will cross the cell membrane (passively or actively) at a flow Q_g, depending on drug permeability and villous blood flow (see S3 Appendix), to join the blood circulatory system. Once the drug is in the blood, it goes to the liver through the portal vein.

https://doi.org/10.1371/journal.pone.0183794.g004

blood flows used for the simulation are taken as the average value of a 70 kg man and are summarized in S1 Table

Numerical resolution

To resolve the herein PBPK, a program was written in MATLAB® R2015b [18], using an object-oriented programming (OOP) approach. First, each compartment was identified as a generic object which generates a function $\boldsymbol{f_i}$ such as $\frac{d\boldsymbol{Y}_i}{dt} = \boldsymbol{f}(t, \boldsymbol{Y}_i)$ where $\boldsymbol{f_i}$ and $\boldsymbol{Y_i}$ are both column vectors and represent the dynamics of the system and variables of interest (*e.g.* blood concentration and enzyme level) of the compartment *i*, respectively. Then, the compartments are combined in a larger object that connects them with their respective blood flows; used to identify the source term for each compartment, and generate a generic function $\boldsymbol{f}(t, \boldsymbol{Y})$ such as $\frac{d\boldsymbol{Y}}{dt} = \boldsymbol{f}(t, \boldsymbol{Y})$ where $\boldsymbol{f}^{tr} = (\boldsymbol{f}_1^{tr}, \boldsymbol{f}_2^{tr}, \ldots, \boldsymbol{f}_n^{tr})$ and $\boldsymbol{Y}^{tr} = (\boldsymbol{Y}_1^{tr}, \boldsymbol{Y}_2^{tr}, \ldots, \boldsymbol{Y}_n^{tr})$. Finally, $\boldsymbol{Y}$ is resolved by using the solver `ode15s`, which was the preferred solver as it can solve stiff problems and adapt the time step for optimum resolution. A more detailed description of the main architecture of the program can be found in the appendix S6 Appendix and the code with an example in appendix S1 Code.

Parameters

Clinical studies. Ten clinical studies, summarized in Table 2, were selected to assess the predictions from the PBPK model with the observations. For each clinical study, midazolam was used to probe the impact of the perpetrator drug on the CYP3A4 enzyme.

Table 2. Summary of 10 *in vivo* clinical studies used in comparison to the simulations.

Perpetrator	Dosage Regimen (p.o)			Victim	Dosage Regimen (p.o)		Observation		Ref.
	Dose	Numbers	Interval		Dose	Intake Time	Ratio		
	(mg)				(mg)	(h)	AUC [a]	C_{max} [b]	
Azithromycin	500	3 doses	*q.d.*[c]	Midazolam	15	49.5	1.27	1.29	[19]
Cimetidine	400	3 doses	Irregular[d]	Midazolam	15	25	1.35	1.26	[20]
Clarithromycin	500	13 doses	*b.i.d.*[e]	Midazolam	8	144	8.39	3.80	[21]
Diltiazem	60	5 doses	*t.i.d.*[f]	Midazolam	15	25	3.75	2.05	[22]
Ethinyl Estradiol	0.03	10 doses	*q.d.*	Midazolam	7.5	217	1.20	1.16	[23]
Fluconazole	400	1 doses	*q.d.*	Midazolam	7.5	2	3.50	2.50	[24]
Fluoxetine	60 & 20	5 & 7 doses	*q.d.*	Midazolam	10	265	0.84	1.11	[25]
Ketoconazole	400	4 doses	*q.d.*	Midazolam	7.5	73	15.90	4.09	[26]
Pleconaril	400	15 doses	*t.i.d.*	Midazolam	5	112	0.65	0.76	[27]
Rifampin	600	10 doses	*q.d.*	Midazolam	5.5	Multiple[g]	0.12	0.17	[28]

[a]AUC: Area Under the Curve $AUC = \int_0^{+\infty} C(t)dt$

[b]Maximum Concentration: $C_{max} = \max_{t \geq 0} C(t)$

[c]*q.d.*: *quaque die* (once a day)

[d]Intakes at 0, 12 and 24.5 h.

[e]*b.i.d.*: *bis in die* (twice a day)

[f]*t.i.d.*: *ter in die* (three times a day)

[g]Intakes at 118 and 190 h.

https://doi.org/10.1371/journal.pone.0183794.t002

CYP3A4 enzyme. The CYP3A4 enzyme was the enzyme of interest, as it is the main enzyme to metabolize midazolam. The amount of the CYP3A4 enzyme in the liver and intestine was taken as equal to 9.228 μmol [8] and 0.070 μmol [8], respectively. To estimate the concentrations E_0 and E_0^g for CYP3A4, the respective amounts were divided by the total volume of hepatocytes V_h, estimated from the liver model, and the gut wall volume given in S1 Table. The degradation rate constants k_{deg} and k_{deg}^g for CYP3A4 were taken equal to 0.0192 h^{-1} [29] and 0.0288 h^{-1} [29] for the liver and intestine, respectively.

Hepatic clearance. In the PBPK model, three parameters, k_{cat}, $V_{max,2}$ and $V_{max,2}^g$, were introduced. The hepatic blood clearance CL_H can easily be obtained from clinical studies, which represents the clearance due to drug metabolism in the liver with respect to the blood compartment. Therefore, CL_H was corrected to estimate the three parameters. This is done first by estimating the apparent intrinsic clearance CL_{int} assuming a parallel tube model [9], due to the similarity with the herein liver model. Then to correct the impact due to exchange mechanisms between blood and hepatocytes, the metabolic intrinsic clearance CL_{int}^* [30] was calculated. The equations for CL_{int} and CL_{int}^* are:

$$\begin{cases} CL_{int} = -\dfrac{Q_{Liver}}{f_u^b} \ln\left(1 - \dfrac{CL_H}{Q_{Liver}}\right) \\ CL_{int}^* = \dfrac{S_{ex}(P + \rho_{out})CL_{int}}{S_{ex}(P + \rho_{in}) - CL_{int}} \end{cases} \tag{20}$$

where f_u^b and S_{ex} are the blood fraction unbound and the total exchange surface between blood and hepatocytes given by the liver model, respectively. Finally, k_{cat}, $V_{max,2}$ and $V_{max,2}^g$ can be

calculated by:

$$\begin{cases} k_{cat} & = f_{m,3A4} \cdot \dfrac{CL^*_{int} K_{m,1}}{E_0 V_h} \\ V_{max,2} & = (1 - f_{m.3A4}) \cdot \dfrac{CL^*_{int} K_{m,2}}{V_h} \\ V^g_{max,2} & = \dfrac{(1 - f^g_{3A4}) A^g_{CYP} V_{GW}}{(1 - f_{3A4}) A_{CYP} V_h} V_{max,2} \end{cases} \quad (21)$$

where $f_{m,\ 3A4}$ is the fraction metabolized by the CYP3A4 enzyme, A_{CYP} and A^g_{CYP} are the total amount of CYP in the liver and intestine, respectively, and f_{3A4} and f^g_{3A4} are the fraction amount of CYP3A4 in the liver and intestine, respectively. Hepatic and intrinsic clearances $CL_H/CL_{int}/CL^*_{int}$ and fraction metabolized $f_{m,\ 3A4}$ are reported in Table 3, blood fraction unbound f^b_u in Table 4, and fraction amounts f_{3A4}/f^g_{3A4} and CYP amounts $A_{CYP}/\ A^g_{CYP}$ in Table S2 Table.

Renal clearance. The renal clearance values CL_R were obtained from the literature (Table 3). As the renal clearance is expressed with respect to the blood compartment, as it is the case for hepatic clearance, an intrinsic renal clearance $CL_{int,R}$ was calculated by assuming a well-stirred model [9]. The intrinsic renal clearance $CL_{int,R}$ can be expressed as:

$$CL_{int,R} = \frac{R_{BP}}{K_{p,K}} \cdot \frac{Q_K CL_R}{Q_K - CL_R} \quad (22)$$

where Q_K, R_{BP} and $K_{p,K}$ are the kidney blood flow (S1 Table), the blood-to-plasma ratio (Table 4) and the kidney partition coefficient (Table 5), respectively.

Remaining parameters. The partition coefficients for each compartment and drug are found in Table 5. Parameters related to reversible inhibition, MBI and induction are reported

Table 3. Metabolism parameters of the drugs.

Drug	CL_H	$CL_{m,\ int}$	$CL^*_{m\,int}$	K_m	$f_{m,\ 3A4}$	CL_R
	L/h	L/h	L/h	μM		L/h
Midazolam	34.42 [31]	1095.19	1991.20	2.30 [32]	0.96 [33]	0.09 [5]
Azithromycin	33.60[a]	353.81	392.18	150.00 [29]	1.00[b]	9.29[a]
Cimetidine	13.44 [34]	16.22	16.83	10.00[c]	0.00	17.22[a]
Clarithromycin	26.52 [31]	112.47	131.30	50.00[d]	0.80	6.00 [31]
Diltiazem	50.20[a,e]	340.21	375.54	30.00[d]	1.00 [35]	2.88[a]
Ethinyl Estradiol	42.52[a]	1643.00	5334.34	18.00[d]	0.60 [36]	0.00
Fluconazole	0.71 [37],[e]	0.80	0.80	10.00[c]	0.00	1.03[a]
Fluoxetine	40.32 [38]	1083.31	1546.61	10.00[c]	0.00	0.00
Ketoconazole	0.69	50.74 [4]	51.46	1.52 [4]	0.00	0.00
Pleconaril	24.29 [39]	1953.50	4248.41	10.00[c]	0.00	0.00
Rifampin	8.66[a]	50.45	51.17	10.00[c]	0.00	1.68[a]

[a]Average value from PharmapPendium® database: www.pharmapendium.com

[b]DrugBank.

[c]Assumed.

[d]Assumed to be Equal to K_i when $f_{m,\ 3A4}$ is not equal to 0.

[e]The Hepatic Clearance was estimated by: $CL_H = CL_T - CL_R$

https://doi.org/10.1371/journal.pone.0183794.t003

Table 4. Fraction unbound and blood-to-plasma ratio of the drugs.

Drug	f_u^p	f_u^b	R_{BP}	$f_u^{h\,a}$	$f_u^{gw\,a}$
Midazolam	0.0264	0.0400 [34]	0.66 [31]	0.0202	0.0189
Azithromycin	0.7000 [40]	0.1200 [41]	5.83[b]	0.0031	0.0055
Cimetidine	0.8730	0.9000 [34]	0.97 [42]	0.9880	1.0000
Clarithromycin	0.1800 [31]	0.2813	0.64 [42]	0.0122	0.0984
Diltiazem	0.2028	0.2200 [34]	0.92 [43]	0.0173	0.0251
Ethinyl Estradiol	0.0300[c]	0.0355	0.84[b]	0.0039	0.0023
Fluconazole	0.6893	0.8900 [41]	0.77[b]	0.1051	1.0000
Fluoxetine	0.0500	0.0500 [41]	1.00[d]	0.0057	0.0049
Ketoconazole	0.0095 [43]	0.0136	0.70 [43]	0.0075	0.0048
Pleconaril	0.0100[c]	0.0146	0.69[b]	0.0041	0.0019
Rifampin	0.1100[c]	0.1809	0.61[b]	0.3513	0.2234

[a] $f_u^h = \frac{f_u^p}{K_{p,Liver}}$ and $f_u^{gw} = \frac{f_u^p}{K_{p,Kidney}}$

[b] $R_{BP} = h \times K_{p,\,RBC} + 1 - h$ where $h = V_{RBC}/V_{Blood}$ is the hematocrit coefficient.

[c] DrugBank database: www.drugbank.ca

[d] Assumed.

https://doi.org/10.1371/journal.pone.0183794.t004

in Table 6 for each drug, whereas fraction absorbed F_a, absorption constant rate k_a, the hybrid gut wall flow Q_g, and the permeability P for each drug are shown in Table 7. Finally, it is assumed that there is no active hepatocyte uptake or efflux for all drugs considered in this present work (*i.e.*$\rho_{in} = 0$ and $\rho_{out} = 0$).

Table 5. Tissue-to-plasma partition coefficients of the drugs.

Drug	$K_{p,\,RBC}$[a]	$K_{p,\,RB}$[b]	$K_{p,\,Kidney}$	$K_{p,\,Lungs}$	$K_{p,\,Liver}$	$K_{p,\,Gut}$
Midazolam	0.005[c]	0.84 [44]	1.41 [44]	1.61 [44]	1.31 [44]	1.40 [44]
Azithromycin	12.424[c]	77.34[c]	110.75[c]	23.16[c]	226.15[c]	126.72[c]
Cimetidine	0.657[c]	0.74[c]	0.88[c]	0.89[c]	0.88[c]	0.83[c]
Clarithromycin	0.252[c]	1.51[c]	1.02[c]	0.43[c]	1.24[c]	1.83[c]
Diltiazem	0.816[c]	5.39[c]	6.26[c]	1.49[c]	11.76[c]	8.10[c]
Ethinyl Estradiol	0.632[c]	10.93[c]	6.11[c]	1.38[c]	7.73[c]	12.79[c]
Fluconazole	0.467[c]	0.54[c]	0.65[c]	0.63[c]	0.66[c]	0.68[c]
Fluoxetine	1.000[c]	6.31[c]	8.96[c]	1.87[c]	18.28[c]	10.30[c]
Ketoconazole	0.096[c]	1.75[c]	1.01[c]	0.39[c]	1.20[c]	2.00[c]
Pleconaril	0.258[c]	4.65[c]	2.58[c]	0.69[c]	3.22[c]	5.34[c]
Rifampin	0.074[c]	0.46[c]	0.32[c]	0.29[c]	0.31[c]	0.49[c]

[a] RBC: Red Blood Cells.

[b] Estimated by averaging the partition coefficients of the remaining tissues: $K_{p,RB} = \sum_{i=1}^{n} V_i K_{p,i} / \sum_{i=1}^{n} V_i$ (see S5 Appendix for equation development).

[c] Theoretical values estimated using the equations by Rodgers and Rowland. Two formula were used; one for the moderate to strong bases ($pK_a > 7$) and the group 1 zwitterions ($pK_{a,1} > 7$) (Rodgers *et al.* 2005) and the second for acids, neutrals, weak bases ($pK_a < 7$) and group 2 zwitterions ($pK_{a,1} < 7$) (Rodgers *et al.* 2006). The parameters used in these equations are given in S3 and S4 Tables.

https://doi.org/10.1371/journal.pone.0183794.t005

Table 6. Interaction parameters of the drugs.

Drug	Inhibition	MBI		Induction		
	K_i	k_{inact}	K_I	FI_{max}	EC_{50}	EC^*_{50} [a]
	μM	h^{-1}	μM		μM	μM
Azithromycin	150.00 [29]	0.30 [7]	19.00 [7]	1[b]	$+\infty$[b]	$+\infty$
Cimetidine	115.00 [29]	0[b]	$+\infty$[b]	1[b]	$+\infty$[b]	$+\infty$
Clarithromycin	50.00 [29]	3.18 [29]	18.90 [29]	1[b]	$+\infty$[b]	$+\infty$
Diltiazem	30.00 [29]	1.68 [29]	1.15 [29]	1[b]	$+\infty$[b]	$+\infty$
Ethinyl Estradiol	18.00 [7]	2.40 [7]	18.00 [7]	70.00 [7]	20.00 [7]	3.33
Fluconazole	3.40 [29]	0[b]	$+\infty$[b]	1[b]	$+\infty$[b]	$+\infty$
Fluoxetine	8.00 [29]	[29]	0.61 [29]	3.10 [29]	0.54 [29]	0.18
Ketoconazole	0.006 [29]	0[b]	$+\infty$[b]	1[b]	$+\infty$[b]	$+\infty$
Pleconaril	$+\infty$	0[b]	$+\infty$[b]	34.00 [45]	16.40 [45]	3.83
Rifampin	100.00 [29]	0[b]	$+\infty$[b]	34.00 [29]	0.57 [29]	0.54

[a] EC_{50} was corrected to take into account fraction unbound in incubation, permeability and active transport where: $EC^*_{50} = f_{u,inc}\frac{S_{ex}(P+\rho_{in})}{S_{ex}(P+\rho_{out})+CL^*_{int}} \times EC_{50}$, S_{ex} = 10046 dm^2 is given by the liver model and $f_{u,\ inc}$ is calculated theoretically by using the formula by Kilford *et al.* 2008.

[b] Not known as being a reversible inhibitor, MBI inhibitor or inducer. If not a reversible inhibitor $K_i = +\infty$, if not a MBI inhibitor $k_{inact} = 0$ and $K_I = +\infty$ and if not an inducer $FI_{max} = 1$ and $EC_{50} = +\infty$.

https://doi.org/10.1371/journal.pone.0183794.t006

Table 7. Fraction absorbed, absorption constant rate, Q_g and permeability of drug chemicals.

Drug	F_a	k_a	Q_g [a]	P
		h^{-1}	L/h	μm/h
Midazolam	1.00[b]	1.16 [31]	15.44	24228.0 [15]
Azithromycin	0.86 [31]	0.11 [31]	20.51	36000.0[b]
Cimetidine	1.00[b]	1.00[b]	2.57	4468.6 [46]
Clarithromycin	0.55 [47]	1.08 [31]	4.77	7807.8 [48]
Diltiazem	1.00 [8]	1.60 [8]	18.41	36000.0[b]
Ethinyl Estradiol	1.00[b]	1.00[b]	15.13	23635.9 [36]
Fluconazole	0.86 [37]	0.88 [37]	6.23	13646.5 [46]
Fluoxetine	1.00[b]	1.00[b]	22.29	36000.0[b]
Ketoconazole	1.00[b]	1.00[b]	23.34	36000.0[b]
Pleconaril	0.70[c]	1.00[b]	23.31	36000.0[b]
Rifampin	1.00[b]	1.00[b]	19.18	36000.0[b]

[a] $Q_g = \frac{CL_{perm}\frac{Q_V}{f_U^b}}{CL_{perm}+\frac{Q_V}{f_U^b}}$: see S3 and S4 Appendices for more details.

[b] Assumed.

[c] DrugBank database: www.drugbank.ca

https://doi.org/10.1371/journal.pone.0183794.t007

Table 8. Sinusoids length for each level.

Level	Length
	μm
1	344.8
2	185.3
3	92.5
4	46.0
5	22.5
Total	**691.1**

https://doi.org/10.1371/journal.pone.0183794.t008

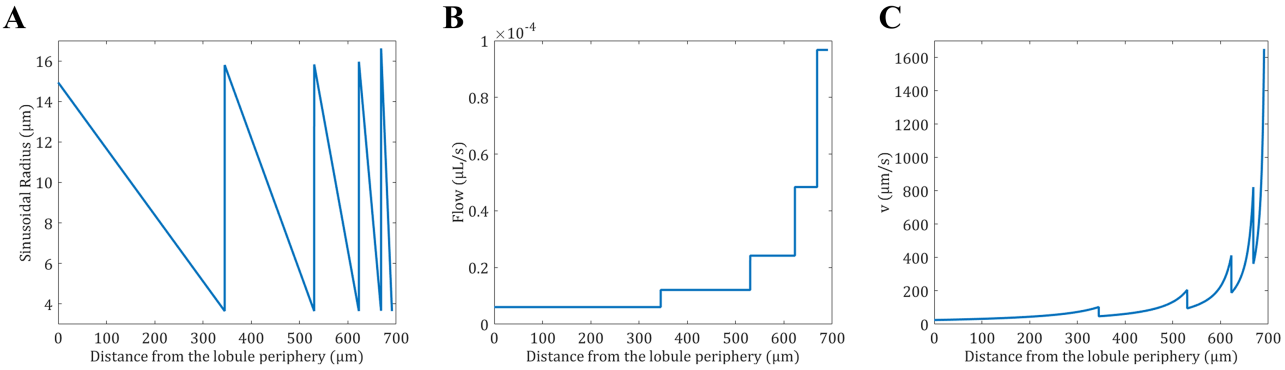

Fig 5. Properties of 5 sinusoid levels from the lobule model. (A) The radius of the sinusoids is expressed as a function of the distance to the periphery of the lobule. For a given level, the radius is decreasing as the sinusoids are converging toward the center of the lobule. Once the sinusoids reach their minimum size they merge together which increases the radius size in a stepwise manner. (B) The flow of the sinusoids is expressed as a function of the distance to the periphery of the lobule. For a given level, the flow is constant, but double when two sinusoids merge. (C) The velocity of the sinusoids is expressed as a function of the distance to the periphery of the lobule. For a given level, the velocity is increasing as the sinusoid radius is decreasing. Once the sinusoids reach their minimum size they merge which decreases the blood velocity suddenly.

https://doi.org/10.1371/journal.pone.0183794.g005

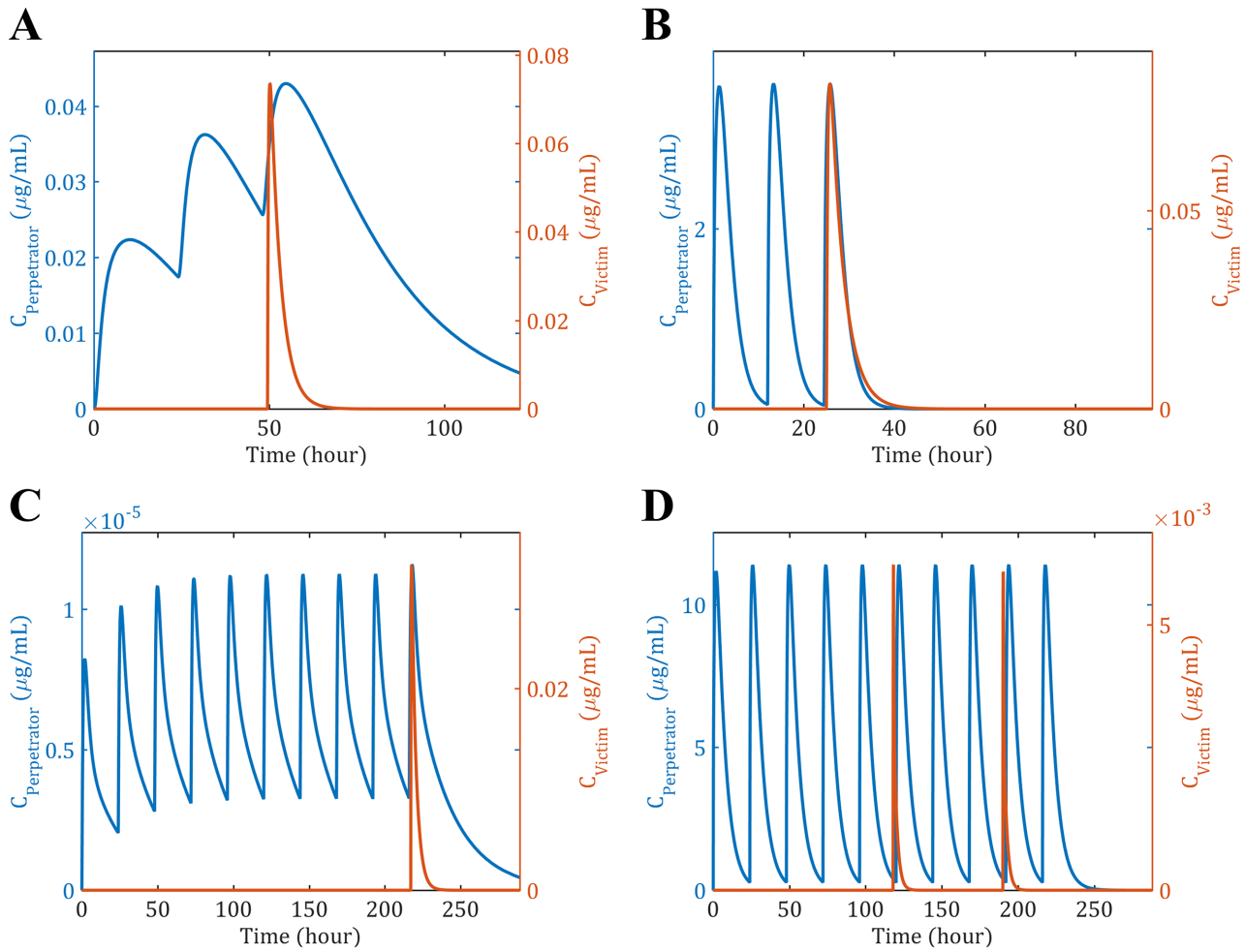

Fig 6. Simulated PK of the perpetrator (blue) and victim (orange) drugs. The simulation were run using the clinical dose regimens from Table 2: (A) Azithromycin (B) Cimetidine (C) Ethinyl Estradiol (D) Rifampin.

https://doi.org/10.1371/journal.pone.0183794.g006

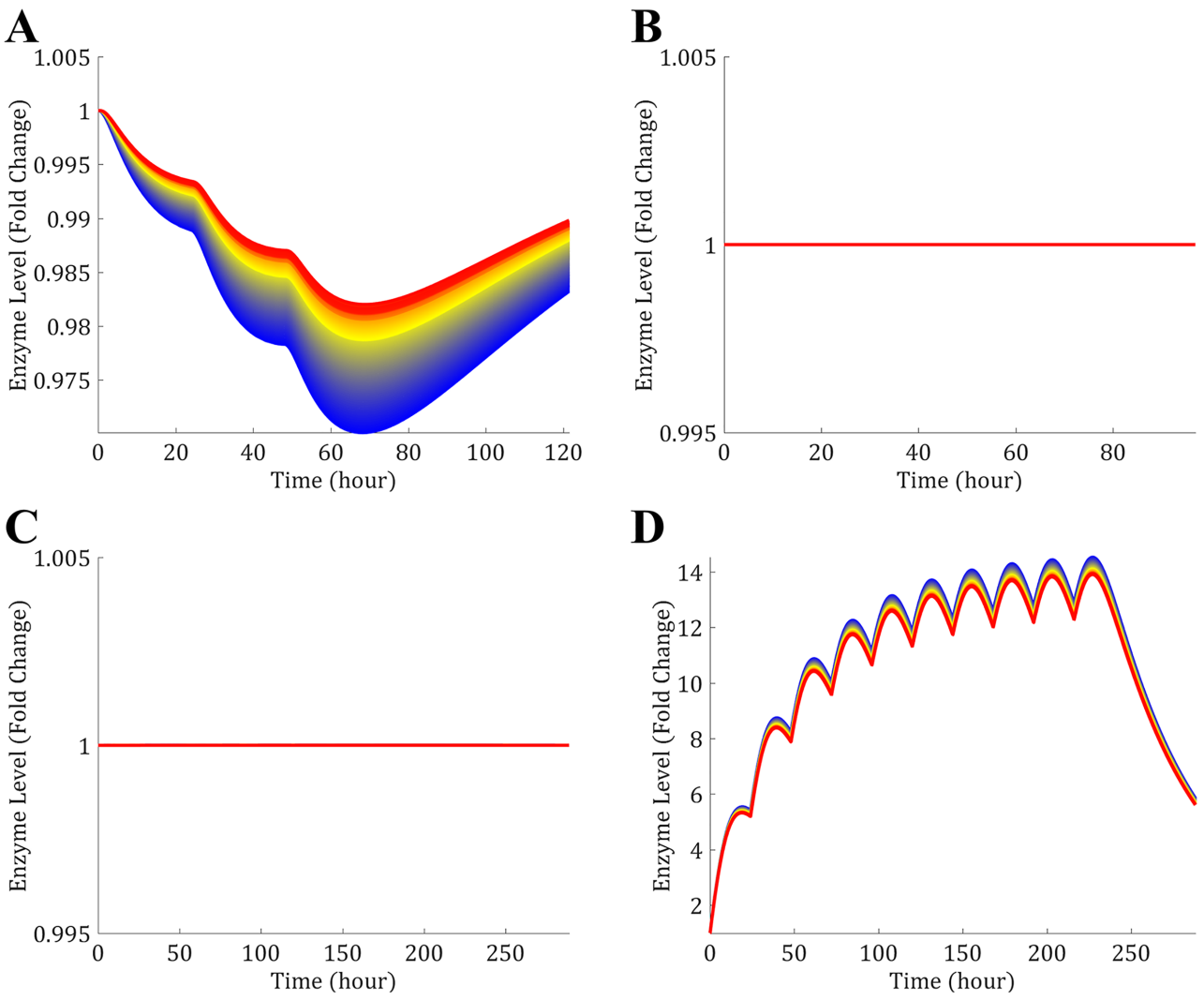

Fig 7. Simulated enzyme levels as a function of time. The total enzyne level (free enzyne + enzyme-substrate complex) is represented as a fold change compared to the initial level. The color gradient indicates the positions within the lobule from blue (Entrance of the lobule) to red (Exit of the lobule): (A) Azithromycin (MBI inducer) (B) Cimetidine (Reversible inhibitor: No effect on enzyme level) (C) Ethinyl Estradiol (MBI inhibitor and inducer: It seems that in this case the effect cancels each other out) (D) Rifampin (Inducer).

https://doi.org/10.1371/journal.pone.0183794.g007

Results

Algorithm construction of liver

The algorithm to construct the lobule geometry generated 5 sinusoidal levels, where the length of each level is represented in Table 8. The volume of one lobule and the number of lobules, estimated from the parameters in Table 1, are respectively 4.06×10^7 μm^3 and 4.16×10^7. Given the average liver volume of 1.69 L for a man of 70 kg (S1 Table), the construction of the lobules respecting the algorithm presented in Fig 1C gave a total hepatocytes volume V_h = 1392 mL and blood volume V_b = 283 mL. Therefore the liver volume given by the model is 1.67 L, which is slightly less than the input volume. Similarly the blood content can be compared to the literature which varies between 250 mL and 312 mL [49]. Furthermore, the surface exchange between blood and hepatocytes S_{ex} given by the model was estimated to be

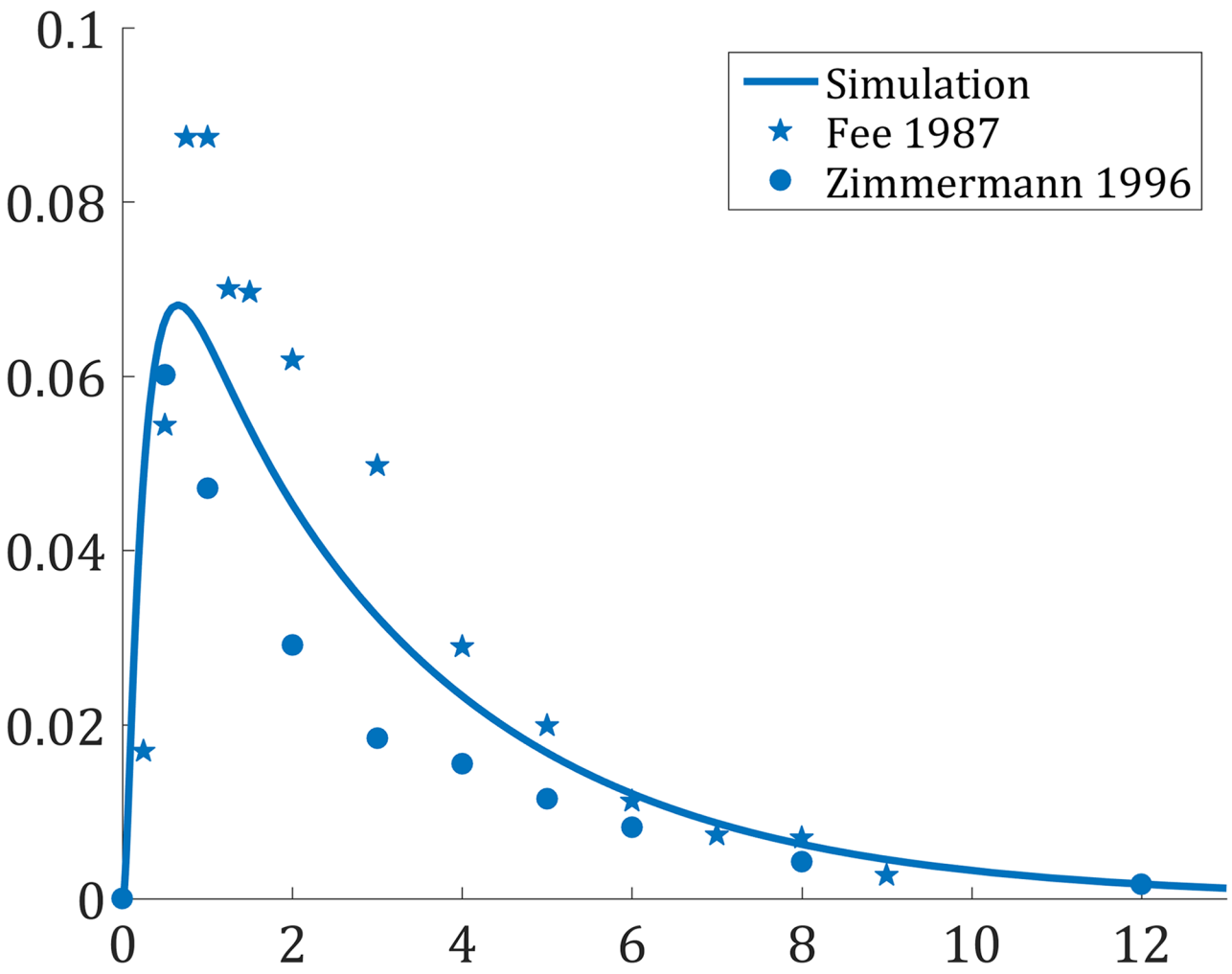

Fig 8. Simulated PK profile for midazolam after an oral dose of 15 mg and comparison to clinical data. (⋆) Fee *et al.* 1987 [20] (•) Zimmermann *et al.* 1996 [19].

https://doi.org/10.1371/journal.pone.0183794.g008

10046 dm^2, which is expected to influence the calculation of CL^*_{int} from *in vivo* data. Finally, assuming a cell volume of V_{cell} = 4 μL/10^6 cells [50], the number of hepatocytes per liver is 348 × 10^9 cells which is equivalent to 193 × 10^6 cells/g of liver. This compares well to the literature values which range from 65 to 185 × 10^6 cells/g of liver [51].

The mathematical construction of the lobule gives the radius of the sinusoids for each level as represented in Fig 5A. Given the number of lobules and the blood flow in the liver, the blood flow for each sinusoid level can be estimated by dividing the total blood flow by the total number of sinusoids at a given level as represented in Fig 5B. From the liver blood flow and the radius of the sinusoids, the velocity in the sinusoids (Fig 5C) was calculated as the ratio of the sinusoids flow to the cross section area as follows: $v(x) = Q(x)/S(s)$, where the cross section area of the sinusoids is expressed as $S(x) = R(x)\ (e_L - 2R_H)$ (see S1 Appendix).

Simulations and comparisons

The clinical data presented in Table 2 were simulated and the PK profiles of the victim and perpetrator drugs are represented in Fig 6. In addition to the PK profiles, the model simulates

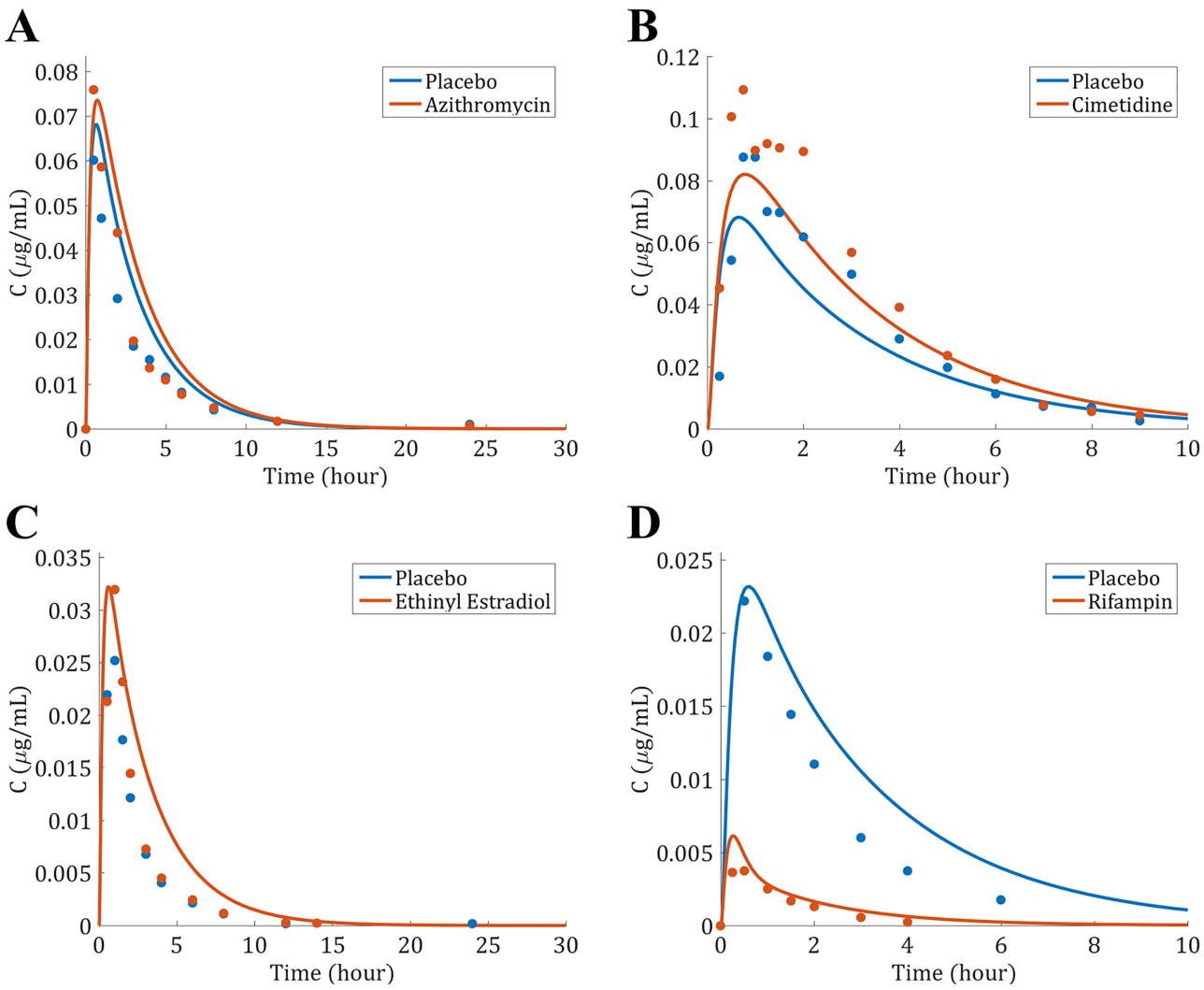

Fig 9. Simulated PK profiles for midazolam with a placebo (blue) or a perpetrator (orange) and comparison to clinical data. The dots represent the clinical observations: (A) Azithromycin [19] (B) Cimetidine [20] (C) Ethinyl Estradiol [23] (D) Rifampin [28].

https://doi.org/10.1371/journal.pone.0183794.g009

the enzyme level in the liver and gut wall as a result of the different mechanisms involved in drug metabolism. The enzyme levels as a function of time in the liver are given in Fig 7, where the spatial effect is also represented with a color gradient. Furthermore, the PK profile of midazolam alone was simulated and compared to clinical data in Fig 8. The model seems to adequately predict midazolam PK. Finally, the PK profiles of midazolam with a placebo and the perpetrator for each of the clinical studies in Table 2 are represented in Fig 9 and a comparison of the prediction and clinical observation of the AUC_{ratio} and $C_{max,ratio}$ are summarized in Table 9. Fold error in eight out of ten predictions are within 2-fold which is a common criteria for good prediction [29, 52]. In Fig 10 the observed AUC_{ratio} are plotted against the predicted AUC_{ratio}. Most of the predictions are relatively well aligned with the line of unity except for the pleconaril scenario where the induction was overpredicted, therefore AUC_{ratio} underpredicted. An R^2 of 0.85 was calculated which indicates a good correlation between the observations and the model predictions.

Table 9. DDI prediction for the 10 clinical studies.

Drug		AUC_{ratio}			$C_{max,\ ratio}$		
Perpetrator	***Victim***	***Observation***	***Prediction***	***F.E.***[a]	***Observation***	***Prediction***	***F.E.***[a]
Azithromycin	Midazolam	1.27	1.16	1.10	1.29	1.08	1.20
Cimetidine	Midazolam	1.35	1.32	1.02	1.26	1.20	1.04
Clarithromycin	Midazolam	8.39	5.36	1.57	3.80	2.24	1.69
Diltiazem	Midazolam	3.75	7.52	2.01	2.05	2.37	1.16
Ethinyl Estradiol	Midazolam	1.20	1.00	1.20	1.16	1.00	1.16
Fluconazole	Midazolam	3.50	4.85	1.38	2.50	2.15	1.16
Fluoxetine	Midazolam	0.84	1.56	1.85	1.11	1.27	1.14
Ketoconazole	Midazolam	15.90	18.17	1.14	4.09	3.09	1.33
Pleconaril	Midazolam	0.65	0.12	5.30	0.76	0.24	3.17
Rifampin	Midazolam	0.12	0.12	1.02	0.17	0.26	1.56
			GMFE[b]	**1.52**		**GMFE**[b]	**1.38**

[a] $Fold\ Error = 10^{\log\left|\frac{Ob}{Pred}\right|}$

[b] GMFE: Geomtric Mean Fold Error $GMFE = 10^{\sum_{i=1}^{N}\log\left|\frac{Ob_i}{Pred_i}\right|}$

https://doi.org/10.1371/journal.pone.0183794.t009

Discussion

The objective of this work was to develop a mathematical model to predict PK drug-drug interactions in a dynamic manner which may occur in the liver and the intestine. The main focus was on the liver, as the majority of drug metabolism and therefore DDIs occur in this organ. However, to incorporate first pass metabolism the intestine was also included. The main results from this work are; (i) the liver model is capable of describing the geometry of a lobule in a simple manner; (ii) the liver model can be incorporated into a PBPK model to predict the PK profile of a drug; (iii) the PBPK model is, so far, capable of predicting the DDIs when one enzyme is mainly involved in DDIs. The novelty of the model presented in this work is the description of the lobule/liver geometry in the simplest manner possible to account for spatial variation in blood flow, concentrations and enzyme level. Furthermore, a cellular model was included to model drug transport, *i.e.* permeability, uptake and efflux, between blood and hepatocytes and drug metabolism within the hepatocytes, without creating a discontinuity with the historical models (*e.g.* the well stirred model [9] or parallel tube model [9]). It has the advantage of comparing the geometrical properties of the lobule generated by the model to physiological data such as the liver blood content, number of lobules, surface exchange, sinusoidal radius, velocity, blood flow profile and, the hydrodynamic pressure load. More detailed geometries have been proposed [14, 53, 54], but their implementation into a pharmaceutical context is not optimal as it is demanding in computational resources (computing power and scientific IT support). Therefore it seems that the liver model herein is an appropriate compromise between the complexity of the model and its implementation. The calculated blood content in the liver (excluding arteries and veins) is in the range of literature values which varies between 250 mL and 312 mL [49]. However, the number of cells per gram of liver is relatively higher than the literature values which range from 65 to 185 $\times 10^6$ cells/g of liver [51]. As it was assumed that the hepatocyte plates are homogeneous, the space of Disse and other cell types (*e.g.* Kupffer cells) were neglected which could have lead to an overestimation of the number of hepatocytes. Based on the lobule geometry, the surface estimated for

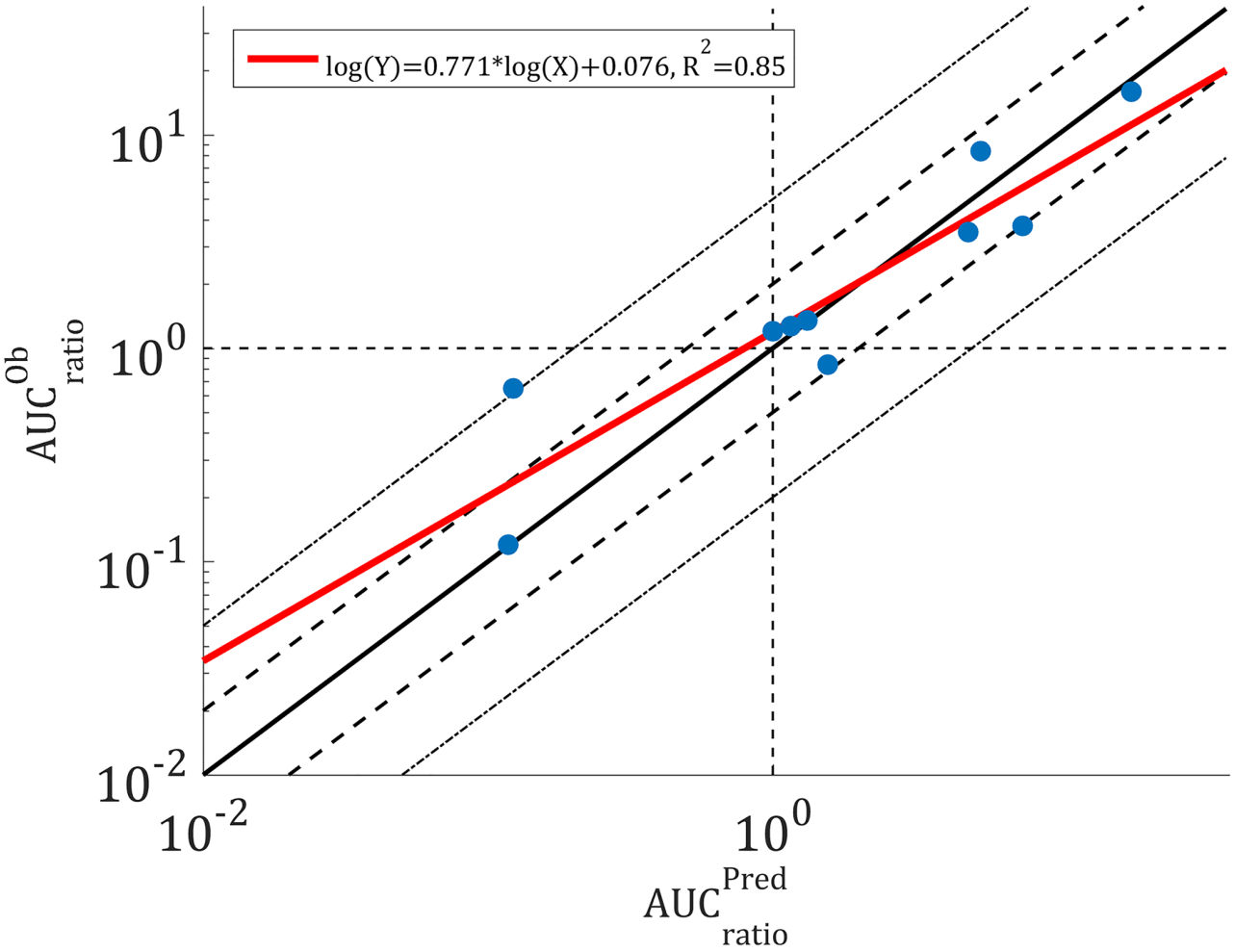

Fig 10. Observed AUC_{ratio} versus predicted AUC_{ratio}. The solid line represents the line of unity, the dashed lines are the 2-fold errors and the dotted lines the 5-fold errors.

https://doi.org/10.1371/journal.pone.0183794.g010

exchanges S_{ex} might have been underestimated as it is half of the maximum surface of exchange; assuming that the surface of all the cells is in contact with blood, which in turn is expected to influence the calculation of the metabolic intrinsic CL^{*}_{int} obtained from *in vivo* data for low permeable drugs. A comparison of *in vivo* and *in vitro* data across a range of drugs may allow to estimate a more realistic value of S_{ex}. Finally, the pharmacokinetic profile of midazolam was relatively well predicted as well as the impact of the perpetrator drug on its *AUC* and C_{max}. Indeed the $GMFE_{AUC}$ was estimated to 1.52 which is in the lower range of literature values (1.47–2.5 [7, 29]). A comparison to the static combined model by Fahmi *et al.* [7] and to a well-stirred model similar to the DDI model by Rowland-Yeo *et al.* [8] was also made (results not shown) where the $GMFE_{AUC}$ were estimated at 2.55 and 1.71, respectively, which suggests that dynamic models are far superior to static models and that geometry might help to improve predictions. However, it is worth noting that the herein results were estimated without taking into account hepatic uptake, which generally improves predictions [55], and without fitting any parameters. All parameters were taken from the literature or calculated using published algorithms. Ideally, each parameter should be estimated experimentally in a specific *in vitro* assays, where it is assumed that they are representative of what is happening *in vivo*.

This point needs careful consideration as measuring the drug-metabolizing ability of isolated hepatocytes leads very often to under-predictions of drug clearance. Moreover, studies have shown that an oxygen gradient [56, 57] and blood flow [58] (*i.e.* shear stress) affect the expression levels of CYPs. The liver model shows that the blood flow inside the liver is non-linear due to its hierarchical anatomical structure and may explain the notion of zonation, *i.e.* CYPs are more highly expressed in certain zones of lobules compared to others. Both effects could be incorporated into the model, where the oxygen concentration and the variation in shear stress, related to changes in velocity in a lobule, can be modeled.

Conclusion

A liver model including a simple description of the lobule geometry and the uptake/efflux transport between the blood and hepatocytes was presented. The model predicts the pharmacokinetic profiles, enzyme activity and drug-drug interaction for different type of DDIs. Future research will test the model with two or more enzymes involved in metabolism to validate the model further, take into consideration uncompetitive, non-competitive or mixed inhibition and potentially add a component for the biliary excretion which is not negligible for some drugs. Furthermore, the model needs to be compared to models with increasing complexity, *i.e.* from static models to dynamic model, to assess how the new features of the herein model improves DDI predictions. Finally, this research focused on the liver as it is the main organ involved in drug metabolism, but the intestine and kidneys may play a significant role in DDIs. Therefore combining the herein liver model to a more sophisticated gut model (*e.g.* the advanced compartmental absorption and transit (ACAT) model) and/or a kidney model, where transporters are taking into account, could potentially improve the prediction of DDIs in the future.

Supporting information

S1 Appendix. The geometry of sinusoids. Description of how the the parameters $\alpha_{B \to H}(x)$ and $\alpha_{H \to B}(x)$ were obtained.
(PDF)

S2 Appendix. Model simplification. Detailed descriptions on how Eqs (10) and (12) were obtain from Eqs (7) and (11).
(PDF)

S3 Appendix. The hybride parameter Q_g. The two definitions of the parameter Q_g by Yang *et al.* [17] and Hisaka *et al.* [16] are presented.
(PDF)

S4 Appendix. Hisaka equation for Q_g. Description of how Q_g is deduced by Hisaka *et al.* [16].
(PDF)

S5 Appendix. Average partition coefficient. Description of how the partition coefficient of a PK compartment composed of different tissues is calculated.
(PDF)

S6 Appendix. Numerical resolution and OOP. A brief description of Object-Oriented Programming (OOP) and a detail description on the program to solve the PBPK model.
(PDF)

S1 Table. Average volume and blood flow for a 70 kg man for different tissues.
(PDF)

S2 Table. Amounts and degradation rate constants for different CYP enzymes in the liver and the intestine.
(PDF)

S3 Table. Physico-chemical properties of the drugs. Physico-chemical parameters used to calculate the partition coefficients.
(PDF)

S4 Table. Composition of human tissue for different organs. Tissue composition used to calculate the partitions coefficient.
(PDF)

S1 Code. Matlab code. The code of all the objects used for the simulations and an example on how to use them to solve a PBPK model.
(RAR)

Author Contributions

Conceptualization: Mohammed H. Cherkaoui-Rbati, Stuart W. Paine.

Data curation: Mohammed H. Cherkaoui-Rbati.

Formal analysis: Mohammed H. Cherkaoui-Rbati.

Funding acquisition: Stuart W. Paine, Cyril Rauch.

Investigation: Mohammed H. Cherkaoui-Rbati.

Methodology: Mohammed H. Cherkaoui-Rbati, Stuart W. Paine, Peter Littlewood, Cyril Rauch.

Project administration: Stuart W. Paine.

Resources: Peter Littlewood.

Software: Mohammed H. Cherkaoui-Rbati.

Supervision: Stuart W. Paine, Peter Littlewood, Cyril Rauch.

Validation: Mohammed H. Cherkaoui-Rbati, Stuart W. Paine, Peter Littlewood, Cyril Rauch.

Visualization: Mohammed H. Cherkaoui-Rbati.

Writing – original draft: Mohammed H. Cherkaoui-Rbati.

Writing – review & editing: Stuart W. Paine, Peter Littlewood, Cyril Rauch.

References

1. Huang SM, Strong JM, Zhang L, Reynolds KS, Nallani S, Temple R, et al. New era in drug interaction evaluation: US Food and Drug Administration update on CYP enzymes, transporters, and the guidance process. J Clin Pharmacol. 2008; 48(6):662–670. https://doi.org/10.1177/0091270007312153 PMID: 18378963
2. Routledge PA, O'Mahony MS, Woodhouse KW. Adverse drug reactions in elderly patients. British Journal of Clinical Pharmacology. 2004; 57(2):121–126. https://doi.org/10.1046/j.1365-2125.2003.01875.x PMID: 14748810
3. U S Food and Drug Administration. Guidance for industry: Drug metabolism/drug interaction studies in the drug development process: Studies in vitro.; 1997. April. Available from: http://www.fda.gov/downloads/AboutFDA/CentersOffices/CDER/UCM142439.pdf.

4. Chien JY, Lucksiri A, Ernest CS, Gorski JC, Wrighton SA, Hall SD. Stochastic prediction of CYP3A-mediated inhibition of midazolam clearance by ketoconazole. Drug Metabolism and Disposition. 2006; 34(7):1208–1219. https://doi.org/10.1124/dmd.105.008730 PMID: 16611859
5. Quinney SK, Zhang X, Lucksiri A, Gorski JC. Physiologically based pharmacokinetic model of mechanism-based inhibition of CYP3A by clarithromycin. Drug Metabolism and Disposition. 2010; 38(2):241–248. https://doi.org/10.1124/dmd.109.028746 PMID: 19884323
6. Einolf HJ, Chen L, Fahmi OA, Gibson CR, Obach RS, Shebley M, et al. Evaluation of various static and dynamic modeling methods to predict clinical CYP3A induction using in vitro CYP3A4 mRNA induction data. Clinical Pharmacology & Therapeutics. 2014; 95(2):179–88. https://doi.org/10.1038/clpt.2013.170
7. Fahmi OA, Maurer TS, Kish M, Cardenas E, Boldt S, Nettleton D. A combined model for predicting CYP3A4 clinical net drug-drug interaction based on CYP3A4 inhibition, inactivation, and induction determined in vitro. Drug Metabolism and Disposition. 2008; 36(8):1698–708. https://doi.org/10.1124/dmd.107.018663 PMID: 18490437
8. Rowland-Yeo K, Jamei M, Yang J, Tucker GT, Rostami-Hodjegan A. Physiologically based mechanistic modelling to predict complex drug-drug interactions involving simultaneous competitive and time-dependent enzyme inhibition by parent compound and its metabolite in both liver and gut—The effect of diltiazem on the time. European Journal of Pharmaceutical Sciences. 2010; 39:298–309. https://doi.org/10.1016/j.ejps.2009.12.002 PMID: 20025966
9. Pang KS, Rowland M. Hepatic clearance of drugs. I: Theoretical considerations of a "well-stirred" model and a "parallel tube" model. Influence of hepatic blood flow, plasma and blood cell binding, and the hepatocellular enzymatic activity on hepatic drug clearance. Journal of Pharmacokinetics and Biopharmaceutics. 1977; 5(6):625–653. PMID: 599411
10. Pang KS, Rowland M. Hepatic clearance of drugs. II: Experimental evidence for acceptance of the "well-stirred" model over the "parallel tube" model using lidocaine in the perfused rat liverin situ preparation. Journal of Pharmacokinetics and Biopharmaceutics. 1977; 5(6):655–680. https://doi.org/10.1007/BF01059689 PMID: 599412
11. Roberts MS, Rowland M. A dispersion model of hepatic elimination: 1. Formulation of the model and bolus considerations. Journal of Pharmacokinetics and Biopharmaceutics. 1986; 14(3):227–260.
12. Roberts MS, Rowland M. A dispersion model of hepatic elimination: 2. Steady-state considerations-influence of hepatic blood flow, binding within blood, and hepatocellular enzyme activity. Journal of Pharmacokinetics and Biopharmaceutics. 1986; 14(3):261–288. https://doi.org/10.1007/BF01106707 PMID: 3783447
13. Tannenbaum C, Sheehan NL. Understanding and preventing drug-drug and drug-gene interactions. Expert Review of Clinical Pharmacology. 2014; 7(4):533–544. https://doi.org/10.1586/17512433.2014.910111 PMID: 24745854
14. Rezania V, Marsh RE, Coombe D, Tuszyński JA. A physiologically-based flow network model for hepatic drug elimination I: Regular lattice lobule model. Theoretical Biology & Medical Modelling. 2013; 10(1):52. https://doi.org/10.1186/1742-4682-10-52
15. Gertz M, Houston JB, Galetin A. Physiologically based pharmacokinetic modeling of intestinal first-pass metabolism of CYP3A substrates with high intestinal extraction. Drug Metabolism and Disposition. 2011; 39(9):1633–1642. https://doi.org/10.1124/dmd.111.039248 PMID: 21632965
16. Hisaka A, Ohno Y, Yamamoto T, Suzuki H. Theoretical Considerations on Quantitative Prediction of Drug-Drug Interactions. Drug Metabolism and Pharmacokinetics. 2010; 25(1):48–61. https://doi.org/10.2133/dmpk.25.48 PMID: 20208388
17. Yang J, Jamei M, Yeo KR, Tucker GT, Rostami-Hodjegan A. Prediction of intestinal first-pass drug metabolism. Current Drug Metabolism. 2007; 8(7):676–684. https://doi.org/10.2174/138920007782109733 PMID: 17979655
18. Matlab. version 8.6 (R2015b). Natick, Massachusetts: The MathWorks Inc.; 2015.
19. Zimmermann T, Yeates RA, Laufen H, Scharpf F, Leitold M, Wildfeuer A. Influence of the antibiotics erythromycin and azithromycin on the pharmacokinetics and pharmacodynamics of midazolam. Arzneimittel-Forschung. 1996; 46(2):213–217. PMID: 8720318
20. Fee JP, Collier PS, Howard PJ, Dundee JW. Cimetidine and ranitidine increase midazolam bioavailability. Clinical Pharmacology & Therapeutics. 1987; 41(1):80–84. https://doi.org/10.1038/clpt.1987.13
21. Gurley B, Hubbard MA, Williams DK, Thaden J, Tong Y, Gentry WB, et al. Assessing the clinical significance of botanical supplementation on human cytochrome P450 3A activity: comparison of a milk thistle and black cohosh product to rifampin and clarithromycin. The Journal of Clinical Pharmacology. 2006; 46:201–213. https://doi.org/10.1177/0091270005284854 PMID: 16432272
22. Backman JT, Olkkola KT, Aranko K, Himberg JJ, Neuvonen PJ. Dose of midazolam should be reduced during diltiazem and verapamil treatments. British Journal of Clinical Pharmacology. 1994; 37:221–225. https://doi.org/10.1111/j.1365-2125.1994.tb04266.x PMID: 8198928

23. Palovaara S, Kivistö KT, Tapanainen P, Manninen P, Neuvonen PJ, Laine K. Effect of an oral contraceptive preparation containing ethinylestradiol and gestodene on CYP3A4 activity as measured by midazolam 1'-hydroxylation. British Journal of Clinical Pharmacology. 2000; 50:333–337. https://doi.org/10.1046/j.1365-2125.2000.00271.x PMID: 11012556

24. Olkkola KT, Ahonen J, Neuvonen PJ. The effects of the systemic antimycotics, itraconazole and fluconazole, on the pharmacokinetics and pharmacodynamics of intravenous and oral midazolam. Anesthesia and Analgesia. 1996; 82:511–516. https://doi.org/10.1097/00000539-199603000-00015 PMID: 8623953

25. Lam YWF, Alfaro CL, Ereshefsky L, Miller M. Pharmacokinetic and pharmacodynamic interactions of oral midazolam with ketoconazole, fluoxetine, fluvoxamine, and nefazodone. The Journal of Clinical Pharmacology. 2003; 43:1274–1282. https://doi.org/10.1177/0091270003259216 PMID: 14551182

26. Olkkola KT, Backman JT, Neuvonen PJ. Midazolam should be avoided in patients receiving the systemic antimycotics ketoconazole or itraconazole. Clinical Pharmacology & Therapeutics. 1994; 55 (5):481–485. https://doi.org/10.1038/clpt.1994.60

27. Ma JD, Nafziger AN, Rhodes G, Liu S, Gartung AM, Bertino JS. The effect of oral pleconaril on hepatic cytochrome P450 3A activity in healthy adults using intravenous midazolam as a probe. The Journal of Clinical Pharmacology. 2006; 46(5):103–108. https://doi.org/10.1177/0091270005283286 PMID: 16397289

28. Chung E, Nafziger AN, Kazierad DJ, Bertino JS. Comparison of midazolam and simvastatin as cytochrome P450 3A probes. Clinical Pharmacology & Therapeutics. 2006; 79:350–361. https://doi.org/10.1016/j.clpt.2005.11.016

29. Fahmi OA, Hurst S, Plowchalk D, Cook J, Guo F, Youdim K, et al. Comparison of different algorithms for predicting clinical drug-drug interactions, based on the use of CYP3A4 in vitro data: Predictions of compounds as precipitants of interaction. Drug Metabolism and Disposition. 2009; 37:1658–1666. https://doi.org/10.1124/dmd.108.026252 PMID: 19406954

30. Shitara Y, Sato H, Sugiyama Y. Evaluation of Drug-Drug Interaction in the Hepatokiliary and Renal Transport of Drugs. Annual Reviews of Pharmacology and Toxicology. 2005; 45:689–723. https://doi.org/10.1146/annurev.pharmtox.44.101802.121444

31. Ito K, Ogihara K, Kanamitsu SI, Itoh T. Prediction of the in vivo interaction between midazolam and macrolides based on in vitro studies using human liver microsomes. Drug Metabolism and Disposition. 2003; 31(7):945–954. https://doi.org/10.1124/dmd.31.7.945 PMID: 12814973

32. Walsky RL, Obach RS. Validated assays for human cytochrome P450 activities. Drug Metabolism and Disposition. 2004; 32(6):647–660. https://doi.org/10.1124/dmd.32.6.647 PMID: 15155557

33. Guo H, Liu C, Li J, Zhang M, Hu M, Xu P, et al. A Mechanistic Physiologically Based Pharmacokinetic-Enzyme Turnover Model Involving both Intestine and Liver to Predict CYP3A Induction-Mediated Drug-Drug Interactions. Journal of Pharmaceutical Sciences. 2013; 102(8):2819–2836. https://doi.org/10.1002/jps.23613 PMID: 23760985

34. Riley RJ, McGinnity DF, Austin RP. A unified model for predicting human hepatic, metabolic clearance from in vitro intrinsic clearance data in hepatocytes and microsomes. Drug Metabolism and Disposition. 2005; 33(9):1304–11. https://doi.org/10.1124/dmd.105.004259 PMID: 15932954

35. Brown HS, Griffin M, Houston JB. Evaluation of Cryopreserved Human Hepatocytes as an Alternative in vitro System to Microsomes for the Prediction of Metabolic Clearance. Drug Metabolism and Disposition. 2007; 35(2):293–301. https://doi.org/10.1124/dmd.106.011569 PMID: 17132764

36. Zhang H, Cui D, Wang B, Han YH, Balimane P, Yang Z, et al. Pharmacokinetic drug interactions involving 17α-ethinylestradiol: A new look at an old drug. Clinical Pharmacokinetics. 2007; 46(2):133–57. https://doi.org/10.2165/00003088-200746020-00003 PMID: 17253885

37. Brammer KW, Farrow PR, Faulkner JK. Pharmacokinetics and Tissue Penetration of Fluconazole in Humans. Reviews of Infectious Diseases. 1990; 12 Supp 3:S318–S326. https://doi.org/10.1093/clinids/12.Supplement_3.S318 PMID: 2184510

38. Schenker S, Bergstrom RF, Wolen RL, Lemberger L. Fluoxetine disposition and elimination in cirrhosis. Clinical pharmacology and therapeutics. 1988; 44(3):353–359. https://doi.org/10.1038/clpt.1988.161 PMID: 3262026

39. Abdel-Rahman SM, Kearns GL. Single-dose pharmacokinetics of a pleconaril (VP63843) oral solution and effect of food. Antimicrobial Agents and Chemotherapy. 1998; 42(10):2706–2709. PMID: 9756781

40. Foulds G, Shepard RM, Johnson RB. The pharmacokinetics of azithromycin in human serum and tissues. The Journal of Antimicrobial Chemotherapy. 1990; 25 Suppl A:73–82. https://doi.org/10.1093/jac/25.suppl_A.73 PMID: 2154441

41. Obach RS, Walsky RL, Venkatakrishnan K, Gaman EA, Houston JB, Tremaine LM. The utility of in vitro cytochrome P450 inhibition data in the prediction of drug-drug interactions. The Journal of

Pharmacology and Experimental Therapeutics. 2006; 316(1):336–348. https://doi.org/10.1124/jpet.105.093229 PMID: 16192315

42. Paixão P, Gouveia LF, Morais JAG. Prediction of drug distribution within blood. European Journal of Pharmaceutical Sciences. 2009; 36(4–5):544–554. PMID: 19152835

43. Yamano K, Yamamoto K, Kotaki H, Takedomi S, Matsuo H, Sawada Y, et al. Correlation between in vivo and in vitro hepatic uptake of metabolic inhibitors of cytochrome P-450 in rats. Drug Metabolism and Disposition. 1999; 27(11):1225–1231. PMID: 10534305

44. Björkman S, Wada DR, Berling BM, Benoni G. Prediction of the disposition of midazolam in surgical patients by a physiologically based pharmacokinetic model. Journal of Pharmaceutical Sciences. 2001; 90(9):1226–1241. https://doi.org/10.1002/jps.1076 PMID: 11745776

45. Fahmi OA, Boldt S, Kish M, Obach RS, Tremaine LM. Prediction of Drug-Drug Interactions from in vitro Induction Data: Application of the Relative Induction Score Approach Using Cryopreserved Human Hepatocytes. Drug Metabolism and Disposition. 2008; 36(9):1971–1974. https://doi.org/10.1124/dmd.108.021907 PMID: 18519654

46. Yee S. In vitro permeability across Caco-2 cells (colonic) can predict in vivo (small intestinal) absorption in man—Fact or myth. Pharmaceutical Research. 1997; 14(6):763–766. https://doi.org/10.1023/A:1012102522787 PMID: 9210194

47. Rodvold KA. Clinical pharmacokinetics of clarithromycin. Clinical Pharmacokinetics. 1999; 37(5):385–398. https://doi.org/10.2165/00003088-199937050-00003 PMID: 10589373

48. Saito H, Fukasawa Y, Otsubo Y, Yamada K, Sezaki H, Yamashita S. Carrier-mediated transport of macrolide antimicrobial agents across Caco-2 cell monolayers. Pharmaceutical Research. 2000; 17(6):761–765. https://doi.org/10.1023/A:1007550820196 PMID: 10955854

49. Snyder WS, Cook MJ, Nasset ES, Karhausen LR, Parry Howells G, Tipton IH. Report of the Task Group on Reference MAN. ICRP; 1975. 23.

50. Paine SW, Parker AJ, Gardiner P, Webborn PJH, Riley RJ. Prediction of the pharmacokinetics of atorvastatin, cerivastatin, and indomethacin using kinetic models applied to isolated rat hepatocytes. Drug Metabolism and Disposition. 2008; 36(7):1365–74. https://doi.org/10.1124/dmd.107.019455 PMID: 18426955

51. Wilson ZE, Rostami-Hodjegan A, Burn JL, Tooley A, Boyle J, Ellis SW, et al. Inter-individual variability in levels of human microsomal protein and hepatocellularity per gram of liver. British Journal of Clinical Pharmacology. 2003; 56(4):433–440. https://doi.org/10.1046/j.1365-2125.2003.01881.x PMID: 12968989

52. Guest EJ, Rowland-Yeo K, Rostami-Hodjegan A, Tucker GT, Houston JB, Galetin A. Assessment of algorithms for predicting drug-drug interactions via inhibition mechanisms: Comparison of dynamic and static models. British Journal of Clinical Pharmacology. 2011; 71:72–87. https://doi.org/10.1111/j.1365-2125.2010.03799.x PMID: 21143503

53. Wambaugh J, Shah I. Simulating microdosimetry in a virtual hepatic lobule. PLoS Computational Biology. 2010; 6(4):e1000756. https://doi.org/10.1371/journal.pcbi.1000756 PMID: 20421935

54. Siggers JH, Leungchavaphongse K, Ho CH, Repetto R. Mathematical model of blood and interstitial flow and lymph production in the liver. Biomechanics and Modeling in Mechanobiology. 2014; 13(2):363–378. https://doi.org/10.1007/s10237-013-0516-x PMID: 23907149

55. Soars MG, Webborn PJH, Riley RJ. Impact of hepatic uptake transporters on pharmacokinetics and drug-drug interactions: Use of assays and models for decision making in the pharmaceutical industry. Molecular Pharmaceutics. 2009; 6(6):1662–1677. https://doi.org/10.1021/mp800246x PMID: 19402709

56. Jungermann K, Kietzmann T. Oxygen: modulator of metabolic zonation and disease of the liver. Hepatology. 2000; 31(2):255–260. https://doi.org/10.1002/hep.510310201 PMID: 10655244

57. Allen JW, Bhatia SN. Formation of steady-state oxygen gradients in vitro: Application to liver zonation. Biotechnology and Bioengineering. 2003; 82(3):253–262. https://doi.org/10.1002/bit.10569 PMID: 12599251

58. Dash A, Simmers MB, Deering TG, Berry DJ, Feaver RE, Hastings NE, et al. Hemodynamic flow improves rat hepatocyte morphology, function, and metabolic activity in vitro. American Journal of Physiology—Cell Physiology. 2013; 304(11):C1053–63. https://doi.org/10.1152/ajpcell.00331.2012 PMID: 23485712